CONTRACT SERIAL NUMBER: 0SQ82-00095

CONTRACTOR: IMPERIAL COLLEGE OF SCIENCE AND TECHNOLOGY, LONDON, ENGLAND

TITLE: Predictive Experiences of CCRL Tunnel Furnace for Powdered Coal Firing

Final Contract Report to Energy, Mines and Resources Canada/CANMET

September 23, 1983

F.C.Lockwood and S.M.A.Rizvi

Imperial College of Science and Technology
London, England

DSS File:18SQ.23440-2-9026
DSS Contract Serial Number:0SQ82-00095
CANMET Scientific Authority: Dr.H.Whaley
CANMET Project Number:434053

MICROMEDIA
63pp

Summary

A prediction procedure developed at Imperial College for powdered coal-fired axisymmetrical combustors is described. It has been used to obtain some predictions of the CCRL tunnel furnace of CANMET which are compared with the experimental data. Prior to these comparisons some tests are performed to assess the sensitivity of the predictions to selected modelling inputs. The physical modelling which we have previously been using at Imperial College appears reasonably suited to the prediction of the CCRL tunnel furnace burning an ALBERTA bituminous coal.

Resumé

Ce papier décrit une methode de calcul d'une chambre de combustion axisymétrique alimentée en charbon pulvérisé, développée à l'Imperial College. Cette methode a été utilisée pour modéliser le four-tunnel "CCRL" de CANMET, et ses résultats sont comparés à des valeurs expérimentales. Auparavant une série de tests a permis d'évaluer la sensibilité de certains parametres de la modélisation. La modélisation physique utilisée jusqu'ici à l'Imperial College semble bien adaptée a la description d'un four-tunnel CCRL alimenté en charbon bitumineux Alberta.

CONTENTS

	Page
SUMMARY	i
LIST OF FIGURES	iv
LIST OF TABLES	vi
INTRODUCTION	1
THE SOLUTION PROCEDURE	2
The Mean Gas Flow Equations Solved	2
The Gas Flow Turbulence Model	3
The Gas Flow Combustion Model	3
Choice of Method for the Coal Particles	4
Handling of the Flow/Particle Interaction	5
The Calculation of Particle Trajectories	7
The Devolatilization Law	8
The Volatiles Combustion Model	12
Dilatation	13
The Char Burn Out Laws	14
Particle Diffusion	16
The Thermal Radiation Model	17
Calculation of Particle Temperature	19
RESULTS OF COMPUTATIONS	20
The CANMET Furnace	20
Furnace Geometry for Sensitivity Studies	21
Operating Conditions for Sensitivity Studies and CCRL Furnace Predictions	21
Effect of Drag Coefficient	27
Effect of Absorption Coefficient	27
Effect of Scattering	28

	Page
Effect of Swelling	28
Effects of Wall Temperature and Emissivities	29
Effect of Char Burn Out Model	29
Effect of Devolatilization Model	30
Comparison with CCRL Data	31
CONCLUSIONS	32
NOMENCLATURE	34
REFERENCES	38

List of Figures

Figure 1 Velocity and scalar grid cells with a particle trajectory

Figure 2 CCRL flame tunnel furnace; geometry and grid

Figure 3 Grid and geometry of a cylindrical combustor used for sensitivity studies

Figure 4 Sensivity to the drag coefficient of radiation heat transfer to cylindrical wall, runs 1 and 2 of Table III

Figure 5 Sensitivity to the absorption coefficient of radiation heat transfer to the cylindrical wall, runs 1 and 3 of Table III

Figure 6 Sensitivity to the scattering factor of radiation heat transfer to cylindrical wall, runs 1 and 4 of Table III

Figure 7 Sensivity to the swelling coefficient of radiation heat transfer to cylindrical wall, runs 1, 5 and 6 of Table III

Figure 8 Sensitivity to the wall temperature and the wall emissivity of radiation heat transfer to cylindrical wall, runs 1, 7 and 8 of Table III

Figure 9 Sensivity to the different char burn out models of radiation heat transfer to cylindrical wall, runs 1 and 9 of Table III

Figure 10 Sensitivity to the different devolatilization models of the radiation heat transfer to cylindrical wall, runs 1, 10, 11 and 12 of Table III

Figure 11 Comparison of predicted and measured radiation heat transfer to the cylindrical wall, CCRL tunnel-furnace, runs 1 and 2 of Table IV

Figure 12 Comparison of predicted and measured gas temperature profiles, CCRL tunnel furnace, run 1 of Table IV

Figure 13 Comparisons of predicted and measured oxygen concentrations profile in CCRL tunnel furnace, run 1 of Table IV

Figure 14 Contours of predicted gas temperature and oxygen concentration, CCRL tunnel furnace, run 1 of Table IV

List of Tables

Table I Specifications of the Coals Used for Sensitivity Studies and Predictions

Table II Specifications of Basic Operating Conditions

Table III Conditions for Sensitivity Studies

Table IV Modelling Conditions for CCRL Tunnel Furnace Comparison

INTRODUCTION

The prediction procedure of this report was originally developed for axisymmetrical gas-fired combustors (e.g. refs. (1) and (2)). It was later extended to powdered coal firing with the aid of sponsorship of the U.K. Central Electricity Generating Board and used to make preliminary sensitivity studies of the various modelling inputs (3). The procedure was subsequently applied to the prediction of coal-fired cement kilns (4), and more recently it has been validated against the long coal flame data of the International Flame Research Foundation (5). The method proved capable of predicting these data with an encouraging degree of success.

The work of the present report is the result of sponsorship for a period of one year by Canada Centre for Mineral and Energy Technology (CANMET). The objectives of the work programme were: to apply the prediction code to the CANMET furnace, to obtain predictions for this furnace which could be compared with data, and to make parametric studies to determine the effect of operating variables. Since the Canadian coals used in the CANMET furnace trials differed from the European coals of previous experience at Imperial College, it was decided that effort should be expended on exploring the sensitivity of the predictions to the physical modelling, and in the sensitive modelling areas to explore new modelling proposals developed for coals other than UK ones. Also, it became clear at an early stage that the many explorations would be facilitated if the economy of the existing code could be enhanced. To this end fairly major modifications were made to the part of the computer code dealing with the velocity and temperature tracking of the char particles.

THE SOLUTION PROCEDURE

The Mean Gas Flow Equations Solved

The main features of the solution procedure are detailed in (3) and (6), a summary only is required here. The basic procedure is comprised of a conventional gas-fired combustor prediction method of the kind of ref. (1) on to which a lagrangian calculation for the particle trajectories, heat and mass transfer, and combustion is superimposed. The present calculations are distinguished from those of (5, 6, 8) by the introduction of swirl, and by a much more economical particle tracking routine.

For the gaseous phase equations are solved of the form:

$$\frac{1}{r}\left[\frac{\partial}{\partial r}(r\bar{\rho}\bar{v}\bar{\phi} + \frac{\partial}{\partial z}(r\bar{\rho}\bar{u}\bar{\phi})\right] = \frac{1}{r}\left[\frac{\partial}{\partial r}\left(\frac{r\mu_{eff}}{\sigma_\phi}\frac{\partial\bar{\phi}}{\partial r}\right) + \frac{\partial}{\partial z}\left(\frac{r\mu_{eff}}{\sigma_\phi}\frac{\partial\bar{\phi}}{\partial z}\right)\right] + \bar{S}_\phi \qquad (1)$$

where r and z are the radial and axial co-ordinates, ρ is density, μ_{eff} is the effective viscosity here calculated by a conventional 'k-ε' turbulence model, σ is a Prandtl/Schmidt number, and the overbars designate time-averaged quantities. The variable ϕ stands for the radial, v, axial, u, and swirl, V_θ, velocities; the specific enthalpy, h_i; the mass fractions of volatile fuel, m_{fu}, oxygen, m_{ox}, and the products of combustion, m_{pr} the turbulence kinetic energy, k; and its dissipation rate, ε. S_ϕ is a source term containing all the influences additional to the convection and diffusion ones, and including the contributions due to the particulate phase. For the case of the swirl velocity which is novel to the present study it is:

$$S_V = -\left(\frac{\bar{\rho v}\,\bar{V}_\theta}{r} + \mu_{eff}\frac{\bar{V}_\theta}{r^2} + \frac{\bar{V}_\theta}{r}\frac{\partial\mu_{eff}}{\partial r}\right) + (\text{the particle momentum transfer of } V_\theta \text{ momentum}) \qquad (2)$$

The Gas Flow Turbulence Model

A standard 'two equation' turbulence model is employed in which modelled balance differential equations for the turbulence kinetic energy, k, and its dissipation rate, ε, are solved (7). The equations run:

$$\rho u \frac{\partial k}{\partial z} + \rho v \frac{\partial k}{\partial r} = \frac{1}{r}\frac{\partial}{\partial r}\left(r \frac{\mu_t}{\sigma_k}\frac{\partial k}{\partial r}\right) + P - \rho\varepsilon \qquad (3)$$

$$\rho u \frac{\partial \varepsilon}{\partial z} + \rho v \frac{\partial \varepsilon}{\partial r} = \frac{1}{r}\frac{\partial}{\partial r}\left(r \frac{\mu_t}{\sigma_\varepsilon}\frac{\partial \varepsilon}{\partial r}\right) + \frac{\varepsilon}{k}(C_{\varepsilon_1}P - C_{\varepsilon_2}\rho\varepsilon) \qquad (4)$$

where the turbulence production P

$\equiv \mu_t\left(\frac{\partial u}{\partial r}\right)^2 + \mu_t\left(\frac{\partial v}{\partial z}\right)^2$, σ_k and σ_ε are Prandtl/Schmidt numbers, $C_{\varepsilon 1} = 1.44$, $C_{\varepsilon 2} = 1.92$, $\sigma_k = 1.0$, $\sigma_\varepsilon = 1.3$ are all empirical constants The turbulent viscosity is determined from:

$$\mu_t = \rho C_\mu k^2/\varepsilon$$

where $C_\mu = 0.09$ is a further empirical constant.

The Gas Flow Combustion Model

The experiments considered here involve diffusion flames. The mathematical description of diffusion flames is normally and considerably assisted (e.g. 9) by three uncritical assumptions that the fuel and oxygen unite in their stoichiometric proportions in the absence of intermediate species to produce one final product only; that the effective turbulent mass diffusion coefficients for the fuel and oxygen are equal; and that the reaction rate is much faster than the physical mixing rate.

The first two of these assumptions determine a conserved scalar (9):

$$\phi = \gamma m_{fu} - m_{ox} \qquad (5)$$

where m_{fu} and m_{ox} are the mass fractions of fuel and oxygen and γ is the fuel/oxygen stoichiometric coefficient.

It is convenient to work with a dimensionless ϕ termed the mixture fraction:

$$f \equiv (\phi - \phi_o)/(\phi_1 - \phi_o) \qquad (6)$$

where the subscripts 1 and o denote the respective values in the fuel stream and in the air. The third of the above assumptions permits piecewise linear relations to be found linking the mass fractions of fuel, oxygen and product to the mixture fraction. These tactics are established and the reader is referred to (9). Standard thermodynamic relations complete the combustion model.

Choice of Method for the Coal Particles

Two approaches for handling the coal particles have been proposed and are conveniently termed Eulerian and Lagrangian. In the former due to Spalding (10), the particle size distribution is represented by a discretisation into uniform-diameter groups with "species-like" partial differential equations being solved for the mass fraction of particles in each group.

In the Lagrangian treatment, formulated by Megdal and Agosta (11), the flights of statistically representative particles are tracked through the combustion chamber from entry to exit. The presence of the particles is made known to the flow code by way of sources of mass, momentum, and energy. This approach has been used by Crowe (12) to solve a spray cooling problem.

There are three principal advantages weighing in favour of the Lagrangian and against the Eulerian treatment: particle slip in

the fluid is very much more easily accounted for; the computer storage requirement does not increase with the number of particle-size groups (as is the case in the straightforward application of the Eulerian approach); and the drag, heat transfer, devolatilisation and other laws which govern the particle behaviour are more readily and obviously applied. Opposing the choice of the Lagrangian treatment is the fact that the turbulence diffusion of the particles is less easily handled, and the fact that the Lagrangian-based computations may be less stable because of the source terms imposed on the mean-flow equations.

In the light of all of these arguments and, because furnace computations can all too readily become prohibitively expensive, placing particular emphasis on its lack of a large storage requirement, we favour the Lagrangian approach. Others may choose to disfavour it, but should they do so it will be for reasons we have failed to identify.

Handling of the Flow/Particle Interaction

The procedure for handling the flow/particle interaction was termed the particle source in cell (PSIC) method for Megdal and Agosta. The cells are the finite-difference control volumes of the gas-phase flow calculations. The presence of a coal particle in a cell is made known to the gas-phase calculations through the application of source terms to the mean flow equations. This is illustrated by the following examples: devolatilisation or burning results in a mass source being applied to the gas-phase continuity equation; the drag force on the particle is reflected in the gas-phase calculations

as a source of momentum; heat transfer between the particle and gas is recognized by an enthalpy source; while burning results in sources being applied to the species conservation equations.

By way of illustration we may write the mass conservation equation as

$$G_n - G_s + G_e - G_w - \Delta M_p = 0 \tag{7}$$

where the G_n, G_s, etc. stand for the mass flow rates of gas across for convenience, the "north", "south", etc. faces of the control volume and ΔM_p is the net mass efflux rate in the gas phase from the coal particles into the cell. Similarly, considering the conservation of any property ϕ, the r direction velocity for example, in the case of momentum conservation in that direction, we may write

$$-M_w^\phi + M_e^\phi - M_s^\phi + M_n^\phi - \Delta M_p^\phi = S^\phi \tag{8}$$

where the M's represent the total fluxes, convective plus diffusive, across each of the control volume faces; S^ϕ stands for any conventional-source term such as the pressure gradient when ϕ is a velocity; and ΔM_p^ϕ is the net efflux of ϕ into the gas phase due to the particles which, again considering ϕ standing for velocity and for particles travelling faster than the gas, would take the form of a positive momentum source.

The hybrid calculation of the elliptic flow field is iterative and entails the following principal steps: i) the computation of the gaseous field variables from guessed initial conditions and assuming no particles; ii) the computation of the particle trajectories from an appropriate drag law for the prevailing gas velocities; iii) the calculation of the particle source terms, i.e. the ΔM_p^ϕ's, for each cell; iv) the recomputation of the gas field under the influence of the particle source terms; v) the returning to step ii) until convergence is achieved.

The Calculation of Particle Trajectories

The particle motion is described by:

$$\frac{du_p}{dt} = -\alpha(\bar{u}_p - \bar{u}_g) \tag{9a}$$

$$\frac{dv_p}{dt} = -\alpha(\bar{v}_p - \bar{v}_g) + \frac{\bar{V}^2_{\theta,p}}{r_p} \tag{9b}$$

$$\frac{d\bar{V}_{\theta,p}}{dt} = -\alpha(\bar{V}_{\theta,p} - \bar{V}_{\theta,g}) - \frac{v_p \bar{V}_{\theta,p}}{r_p} \tag{9c}$$

where the subscripts p and g are introduced to distinguish particle from gas quantities, α is defined as $(18\mu C_D Re/24)/(\rho_p d^2)$. We take $C_D = ((1.0 + 0.15Re^{0.687})/Re/24)$. The conventional Reynolds averaging implied by these equations introduces additional turbulence correlation terms (13) which we have ignored along with the gravitational effects. The particle turbulence dispersion is approximately accounted for by the use of corrective 'drift' velocities (3).

The particle tracking procedure has been simplified compared with that of (5, 6, 14 and 15) resulting in a major improvement in economy for equivalent accuracy. Refer to Fig. 1 which shows a sketch of a typical portion of the staggered grid. Equations 9 are integrated by straightforward finite-differencing for a time step Δt. In practice it is found that good precision is typically procured for a Δt which is large enough to give a distance increment of the order of the local cell dimensions.

In the sketch, the particle moves between positions 1 and 2 in the time increment Δt. If the change in particle u-directed momentum in this time is $M_{u,p}$, then the amount which is transferred to the gaseous phase in the u-velocity cell is:

$$M_{u,g} = \frac{\Delta t_1 + \Delta t_2}{\Delta t} M_{u,p}$$

Similarly for the v-velocity cell we have:

$$M_{u,g} = \frac{\Delta t_1}{\Delta t} M_{u,p}$$

And for the transfer of a scalar quantity we write:

$$M_{\phi,g} = \left(\frac{\Delta t_1 + \Delta t_2 + \Delta t_3}{\Delta t}\right) M_{\phi,p}$$

So, in contrast to our previous practice, the particle trajectories are straightforwardly calculated without particular regard to the location 1, 2, ..., and the sources apportioned among the gaseous cells.

The Devolatilization Law

Several proposals have been made to describe the release of volatiles when a coal particle is heated. The ones we have examined are summarized below. In general the rate of volatiles release is a function of the particle temperature, its rate of change of temperature, the fineness of grind, and the coal type. Clearly the quest for a universal model formulation is a difficult one. The hope is that the predictions will not be critically dependent on the detailed features of and parameter prescription of the model.

(i) Constant evaporation rate model

In this simple model suggested by Baum and Street (16) a constant devolatilization rate is assumed, the value of which is adjusted to the experimental data. Rate of volatile released is:

$$\left(\frac{d}{dt}\right) X_V = B \qquad (10)$$

where X_V is the fraction of total volatiles (based on the proximate analysis) released and B is the devolatilization-rate constant which on the basis of previous experience we have taken as 30.0 in the present studies (3, 17).

(ii) Single reaction model

The overall volatile release process is approximated as a first-order decomposition occurring uniformly throughout the particle. The rate of devolatilization is expressed as:

$$\frac{dV}{dt} = K(V^* - V) \qquad (11)$$

where V = mass of volatiles evolved/mass of original coal at time t; V^* = the value of V at $t \to \infty$, the ultimate volatile gain; K = rate constant of Arrhenius form = $K_o(\exp(-E/RT))$, s^{-1}; K_o = frequency factor, s^{-1}; E = activation energy, J/Kg mol; T = particle temperature ^oK. Badzioch and Hawksley (18) pointed out that V^* should strictly be distinguished from the volatile matter VM in the coal, determined by proximate analysis. It has now been established that the ultimate yield of the volatiles is generally different from the volatile contents, VM, of the coal. The ratio V^*/VM varies from 0.75 - 1.36 for several American, British and French coals (19). For the Pittsburgh Seam Bituminous coal used in the present model sensitivity studies following values are assumed (20). $E = 0.494 \times 10^8$ J/Kg.mol; $K_o = 706\ s^{-1}$; $V^* = 48.4$ of the original coal (at 1 atm and for a heating rate of $10^4\ ^oC/s$).

(iii) Two-competing reaction scheme (Kobayashi et al (21))

This model is based on the concept of two competing overall reactions, the rate of each differing principally due to temperature:

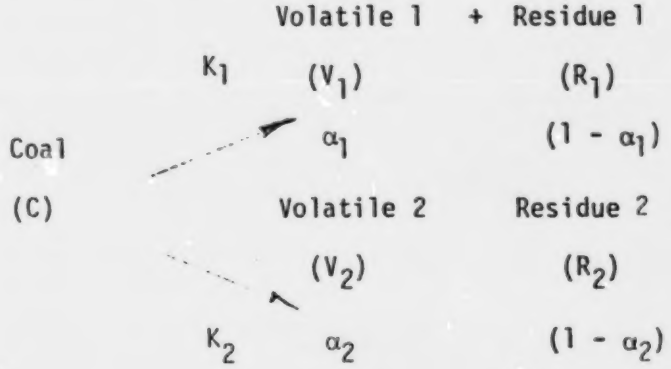

Where α_1 and α_2 are mass stoichiometric coefficients. The rate constants K_1 and K_2 are given by

$$K_1 = B_1 \exp(- E_1/RT)$$

$$K_2 = B_2 \exp(- E_2/RT)$$

Where B_1 and B_2 are frequency factors and E_1 and E_2 are the activation energies for the respective reactions. The first reaction is assumed to be dominant at low temperatures with the volatile yield of α_1 and the second reaction is more effective at high temperatures and the yield is α_2. It therefore implies that the activation energy of second reaction E_2 is much higher than E_1, the activation energy of first reaction. The overall weight loss can therefore be written as:

$$V = \int_0^t [\alpha_1 B_1 \exp(- E_1/RT) + \alpha_2 B_2 \exp(- E_2/RT)] \times \exp\left[- \int_0^t [B_1 \exp(- E_1/RT) + B_2 \exp(- E_2/RT)]dt\right]dt \qquad (12)$$

For the Pittsburgh Seam coal, the values of the constants are assumed as (21): $\alpha_1 = 0.30$, $\alpha_2 = 1.0$, $B_1 = 2.0 \times 10^5\ s^{-1}$, $T_{a1} = (E_1/R) = 12630\ ^oK$, $T_{a2} = (E_2/R) = 20200\ ^oK$.

(iv) Multiple parallel devolatilization model of Anthony et al (20)

It is assumed that the thermal decomposition of a coal molecule is described by a large number of independent chemical reactions, with different chemical bond strength. Taking the decomposition of one particular reaction (denoted by i) as:

$$\frac{dV_i}{dt} = K_i(V_i^* - V_i) \tag{13}$$

Where K_i is of the Arrhenius form, integration of the above equation gives, for $K_i = K_o \exp(- E_i/RT)$:

$$V_i^* - V_i = V_i^* \exp(- K_o t \exp(- E_i/RT)) \tag{14}$$

It is assumed that K_i's differ only in activation energies E_i (that is $K_{oi} = K_o$ for all i) and that the number of reactions is large enough to permit E to be expressed as a continuous distribution function f(E), with f(E)dE representing the fraction of the potential volatile loss V* which has an activation energy between E and E + dE. V_i^* can then be written as:

$$dV^* = V^* f(E)dE$$

$$\text{with} \qquad \int_o^\infty f(E)dE = 1 \tag{15}$$

The total volatile yield can then be written as:

$$\frac{V^* - V}{V^*} = \int_o^\infty \exp\left[- K_o t \exp(- E/RT)\right] f(E)dE \tag{16}$$

If f(E) is assumed to be a Gaussian distribution with a mean activation energy of E_o and a standard deviation σ, of the form:

$$f(E) = \left[\sigma \sqrt{2\pi}\right]^{-1} \exp\left[- (E - E_o)^2/2\sigma^2\right], \tag{17}$$

Then the volatile content can be expressed as:

$$V = V^* - \frac{1}{\sqrt{2\pi}} \int_o^\infty \left[1 - \exp(- \int_o^t K_o \exp(- \frac{E}{RT})dt\right] x \exp\left[- \frac{(E - E_o)^2}{2\sigma^2}\right] dE \tag{18}$$

Where for the Pittsburgh coal: V* = total yield (% of Wt. of original coal) = 48.4, see (20); E_o = mean activation energy = 2.12×10^8 J/Kg mol; $K_o = 1.67 \times 10^{13}$ sec^{-1} (frequency factor); σ = standard deviation of activation energy 2.93×10^7 (J/Kg/mol).

The Volatiles Combustion Model

The release of volatiles is a rapid process displacing any surrounding oxygen and products away from the particles. As a result it is very unlikely that the volatiles will burn in the immediate vicinity of the particle. Their combustion is much more likely to occur during or after mixing with surrounding gases at a rate determined, not by chemical kinetic considerations, but by the turbulence dissipation rate in the gas phase. An economic phenomenological model is required for the general case of partially premixed turbulent combustion and we have chosen the one due to Magnusen and Hjertager (22).

These authors assume, in the same manner as Spalding (23) in his original "eddy break up" model, that the turbulence decay rate, and so the reaction rate, is proportional to the time scale of the large-scale eddies as characterized by the ratio ε/k. They further assume the reaction rate is also proportional to the smallest of the fuel, oxygen, or products concentrations and write:

$$R_{fu} = \left[\bar{\rho}A\bar{m}_{fu}\frac{\varepsilon}{k},\ \frac{\bar{\rho}A\bar{m}_{ox}}{s}\frac{\varepsilon}{k},\ \bar{\rho}A'\frac{m_{pr}}{1+s}\frac{\varepsilon}{k}\right] \qquad (19)$$

where R_{fu} is the volumetric reaction rate of fuel, $\bar{\rho}$ is the time-averaged density, s is the stoichiometric oxygen requirement by mass, $\bar{m}_{fu}$, $\bar{m}_{ox}$ and $\bar{m}_{pr}$ are respectively the time-averaged mass fractions

of fuel, oxidant, and products, and A = 4 and A' = 2 are empirical constants, the lack of universality of the model being reflected in the need for two constants instead of one.

Dilatation

The escape of the volatile matter usually causes a dialation of particle size. The extent of this depends on the type of coal and the combustor conditions. Therefore all the complex and interrelated factors which affect devolatilization also affect the particle swelling. Since the particle drag, convective heat and mass transfer, kinetic burning rate and radiation exchange are all affected by swelling it emerges as an important modelling parameter. Fortunately the swelling factor (defined as the particle diameter after volatile release/the raw coal particle diameter) seems not to be large. Street et al (16) report values between 1.04 and 1.1.

Adjustment of the assumed swelling factor is a convenient method of obtaining agreement between predictions and data. Baum and Street (16) have suggested this in their paper. Indeed, we have found it a necessary artefact to procure the optimum performance of particle burning model of Field et al (24). Obviously a self consistent model which accommodates a realistic swelling factor is preferable.

The Char Burn Out Laws

The particle burning rate may be expressed as:

$$R_c = \Gamma_{ox}(m_{ox,\infty} - m_{ox,o}) = k_c \dot{m}^n_{ox,o} \qquad (20)$$

where k_c is the chemical rate coefficient and n is the reaction order. For n = 1, for example, we get:

$$R_c = m_{ox,\infty}/(1/\Gamma_{ox} + 1/k_c) \qquad (21)$$

which illustrates the competition between the diffusional and chemical rates. The measured chemical rate coefficient will in general be a function of: the actual rate constant for the char/oxygen reaction, and internal regions of the particle; the amount of reaction surface; and the freedom of access of the oxygen to the internal pore structure.

Various researchers (25,26,27,28) have identified three 'zones' of burning rate control during the combustion of a porous particle.

Zone I: Here the burning rate is controlled by the chemical reaction only, and the relatively faster diffusion provides oxygen to the internal and external particle surfaces at bulk gas concentration. For this case $\Gamma_{ox} >> k_c$.

Zone II: As the reaction rates increase at higher particle temperature, the oxygen concentration at the surface and within the pores is lowered below the bulk gas concentration and zone II conditions are reached. For this case Γ_{ox} and k_c are of the same order.

Zone III: For still higher particle temperatures the reaction rate is fast enough to consume most of the oxygen near the particle surface and the burning rate is limited by the transport of oxygen across the boundary layer to the particle surface. For this case $k_c < \Gamma_{ox}$ and a much weaker temperature dependence is observed under these conditions.

We have considered two char burn out models in the present

(i) Model of Mitchell and McLean

Mitchell and McLean (29) made least square fits to the data for a bituminous Millmerran Char (Australian) under zone II and transition to zone III conditions. Their least squares fit to the overall burning rates per unit external surface area is given by:

Zone II: $R_c = 32.3 \exp(-7.828 \times 10^7/RT_p)$ $Kg/m^2 \cdot sec$ (22)

Transition to Zone III: $R_c = 20 \times 10^{-6} T_p^{1.16}$ $Kg/m^2 \cdot sec$ (23)

The transition to zone III for Millmerran coal is observed at about 1725^oK. The authors state that this coal does not burn under zone conditions.

For the present study, due to lack of appropriate data and because the analyses are not too different, the above rate of burning was assumed for the Pittsburgh seam bituminous coal of the present sensitivity studies.

(ii) Model of Field et al

Field et al (24) express the burning rate as:

$$\frac{dM_p}{dt} = - K_T \pi d_p^2 p F_{ox} \quad (24)$$

We have retained their notation here and M_p and d_p are the particle mass and diameter, respectively, F_{ox} is the volume fraction of oxygen at its surface, p is the pressure, and K_T is an overall rate coefficient defined by:

$$K_T = (K_{ch} \cdot K_{ph})/(K_{ch} + K_{ph}) \quad (25)$$

where K_{ph} and K_{ch} are the diffusion and chemical rate coefficients, respectively. These latter are given by:

$$K_{ph} = 4D_c M_c \phi'/[Rd_p(T_p + T_g)]. \quad (26)$$

and

$$K_{ch} = A_f \psi' \exp(- E/RT_p) \qquad (27)$$

Here D_c is the diffusion coefficient taken as $= T_{ox}$; M_c is the atomic weight of carbon, ϕ' is a mechanism factor, R is the universal-gas constant, T_p and T_g are the particle and gas temperatures, A_f is a frequency factor, ψ' is a surface factor, and E is the activation energy.

We have further considered the burning rate recommendations in the comprehensive review paper by Smith (28). These cover a wider range of coals and are based on single particle experiments burning in pure oxygen. Unfortunately we have found that they do not seem to permit reliable extension to the much lower oxygen concentrations in a furnace and burning rates of the wrong size are frequently encountered. The application of this otherwise useful information requires further consideration. The difficulty of ascertaining general models for the complex phenomena of char combustion is again emphasized.

Particle Diffusion

The particle trajectory depends not only on the mean gas-phase velocity but in reality it must also be a function of the velocity fluctuations. The turbulence has the effect of dispersing or diffusing the particles to an extent dependent on the ratio of the particle diameter to the turbulence integral scale. For very large values of this

parameter (approaching 0.1 say) the particle migrations will be negligible, whereas for very small values their excursions will be of the same order as the integral length scale. Intermediate values of the parameter are expected to characterize typical PF flames. The modelling of the turbulent diffusion of particles is a very challenging and insufficiently explored subject. We have adopted the following simple expedient.

The diffusional velocities are calculated from:

$$V_{diff} = C_1 \, |\overline{v'^2}| \tag{28a}$$

and

$$U_{diff} = C_2 \, |\overline{u'^2}| \tag{28b}$$

where C_1 and C_2 are empirical constants. The turbulence gas velocity fluctuations are estimated with the aid of the Boussinesq hypothesis:

$$\overline{v'^2} = - C_3 \frac{2\mu_t}{\rho}(d\bar{v}/dr) + \frac{2}{3} k \tag{29a}$$

$$\overline{u'^2} = - C_4 \frac{2\mu_t}{\rho}(d\bar{u}/dx) + \frac{2}{3} k \tag{29b}$$

where C_3 and C_4 are further empirical constants of order unity. The mean trajectory is now computed by substituting in eq. (9) $u_p = \bar{u}_p + U_{diff}$ and $\bar{v}_p = \bar{v}_p + V_{diff}$.

The Thermal Radiation Model

We assume a grey system in which case the attenuation of intensity I with distance s_Ω in the direction Ω may be expressed by:

$$\frac{dI}{ds_\Omega} = - k_g(I - \frac{E_g}{\pi}) - (\varepsilon_p A_p + r_p A_p)I + \varepsilon_p A_p \frac{E_p}{\pi}$$

$$+ \frac{r_p A_p}{4\pi} \int_{4\pi} p(\Omega,\Omega') I(\Omega') d\Omega' \tag{30}$$

where $E \equiv \sigma T^4$, k_g is the gas absorption coefficient, ε_p and r_p are the particle emissivity and reflectivity, respectively, A_p is the total projected area of the particles per unit volume, and $p(\Omega,\Omega')$ is the probability that incident radiation in the direction Ω' will be scattered into the element of solid angle $d\Omega$.

The above transfer equation is approximately, but probably adequately, handled by the moment method due to Gibb (30) which results in the following "flux type" equations:

$$- \frac{\partial}{\partial x_i}\left(\frac{1}{3k_e}\frac{\partial E_r}{\partial x_i}\right) = k_g(E_g - E_r) + \varepsilon_p A_p(E_p - E_r) \qquad (31)$$

where

$$E_r \equiv \sigma T_r^4 \ , \quad T_r^4 \equiv \frac{1}{4\sigma}\int_{4\pi} I d\omega \ ,$$

and $k_e \equiv k_g + A_p[\varepsilon_p + r_p(1 - f)]$

is an extinction coefficient, and f is a scattering factor which is negative, zero, or positive for respectively backward, isotropic, or froward scattering. Gibb has suggested $\varepsilon_p = 1$ and $r_p = 0$ for the coal particles, $\varepsilon_p = r_p = 0.5$ for the ash particles, and $f = 0.9$ everywhere.

The appropriate wall boundary condition is given by

$$- \frac{1}{3K_e}\frac{\partial E_r}{\partial n} = \frac{1}{2}\frac{(1 - r_w)E_r - \varepsilon_w E_w}{1 + r_w} \qquad (32)$$

where n is a distance normal to the wall and ε_w and r_w are respectively the wall emissivity and reflectivity.

Calculation of Particle Temperature

The total heat transfer to the particle per unit mass H_t would be

$$H_t = H_c + H_b + H_r \tag{33}$$

H_c is the heat gained by convection:

$$H_c = Nu\pi d_p K_g (T_g - T_p)/M_p \tag{34}$$

where Nu = Nusselt number, d_p = particle diameter, K_g = gas thermal conductivity, T_g = gas temperature, T_p = particle temperature and M_p = particle mass.

The quantity H_b is the particle heat gained due to burning and is

$$H_b = - h_c (\frac{dM_p}{dt})/M_p \tag{35}$$

where h_c = char calorific value and $(\frac{dM_p}{dt})$ = rate of char burning. We choose to associate all the particle heat release with the particle. In reality some will be transferred to the gas, but the influence of the split will be small.

H_r is the heat gained by the particle due to radiation:

$$H_r = \pi\sigma\varepsilon_p d_p^2 (T_R^4 - T_p^4)/MP \tag{36}$$

The various symbols have been defined in the previous subsection.

The particle temperature is assumed constant throughout its mass and its rate of change is given by:

$$C_p (\frac{dT_p}{dt}) = H_t - \frac{L}{M_p}(\frac{dM_p}{dt}) \tag{37}$$

Where C_p is the particle specific heat and L is the latent heat of volatilization which is set to zero when devolatization is complete. Substituting for H_t in (37) and we have:

$$\frac{dT_p}{dt} = K_1(T_g - T_p) + K_2 + K_3(T_R^4 - T_p^4) \qquad (38)$$

where $K_1 = \pi Nu K g d_p/(M_p C_p)$, $K_2 = -h_c(\frac{dM_p}{dt})/(M_p C_p) + (L/M_p C_p)(\frac{dM_p}{dt})$, and $K_3 = \pi\sigma\varepsilon_p d_p^2/(M_p C_p)$.

Rearranging eq. (38) gives:

$$\frac{dT_p}{dt} = (A - BT_p) \qquad (39)$$

where $A = K_1 I_g + K_2 + K_3 T_R^4$, $B = K_1 + K_3 T_P^3$.

A recurrence relation of the following form can be obtained from solving (39):

$$T_{p_{n+1}} = T_{p_n} e^{-B\delta t} + (A/B)(1 - e^{-B\delta t}) \qquad (40)$$

where $B = (K_1 + K_3 T_{p_n}^3)$ and the locations n and n+1 are a consequence of the finite time increment δt.

RESULTS OF COMPUTATIONS

The CANMET Furnace

The basic geometry of the tunnel furnace is sketched in Fig. 2. It is 5.25 m in length and 0.8 m in diameter. For the runs for which CANMET have provided data the first 1 m of combustion tunnel were refractory lined. The walls of the remainder of the tunnel are cooled by an organic liquid. The burner is a standard double concentric design having the dimensions indicated. The exit opening is 0.3 m in diameter. The computational grid used for the calculations reported herein is sketched on the figure 2.

Furnace Geometry for Sensitivity Studies

The geometry assumed for the parameter sensitivity studied differs slightly from that of the CCRL combustor. This is due to misunderstandings in the early stages of the contract concerning several details of the true CCRL geometry. The assumed geometry is sketched in Fig. 3. Since there is now no upstream length of refractory it was found necessary to raise the wall temperature to achieve a satisfactory burn out. This apparently confirms experience in the real furnace. That the geometry assumed for the sensitivity studies differ from that of the real furnace is of little consequence since the object of these studies was to compare different modelling proposals.

Operating Conditions for Sensitivity Studies and CCRL Furnace Predictions

The sensitivity studies were conducted for a Pittsburgh coal for which model data was available. Experience gained there was transferred to the Alberta coal of the CCRL trials for which the appropriate model constants were otherwise unknown. The specification of these coals is given in Table I.

Table I Specifications of the Coals Used for Sensitivity Studies and Predictions

1. Sensitivity Studies

Pittsburgh Seam no. 8 hv, A-b (Ireland)

Proximate Analysis		Ultimate Analysis	
Volatile matter	% : 40.7	C % :	67.81
Ash	% : 11.07	H_2 % :	5.03
H_2O	% : 2.2	N_2 % :	1.2
Fixed carbon (by diff.)	% : 46.03	S % :	4.14 (by diff.)
		O_2 % :	8.55
		H_2O % :	2.2
		Ash % :	11.07

Calorific value of moisture mineral free coal = 33.474 MJ/Kg.

Stoichiometric air requirement: 9.4 kg/kg

2. CCRL Furnace Prediction

Alberta coal, code name 'E'.

Proximate Analysis (air dried basis)		Ultimate Analysis (air dried basis)	
Volatile matter	: 39.2	C % :	68.88
Ash	: 11.7	H % :	4.73
Fixed carbon	: 49.1	S % :	0.59
		N_2 % :	2.03
		O_2 % :	12.07
		Ash % :	11.70

Calorific value: 28.41 MJ/Kg (dry basis)

Stoichiometric air requirement with 7.8% H_2O in coal: 8.4 kg/kg

The basic operating conditions for the two sets of predictions are presented in Table II. We have noted above that the elevated wall temperature of the sensitivity runs was necessary to ensure good burn out in the absence of upstream refractory. Other inputs for the sensitivity predictions displayed in the Table II were assumed in advance of receiving information from CANMET in the light of previous experience of some run conditions for the furnace of the International Flame Research Foundation.

The 12 basic runs of the sensitivity studies are summarized by Table III. Run 1 represents the base conditions. In the first sensitivity study the drag coefficient, C_d, is altered by 10% from the assumed value (see the definition of α in eq. (9)). Many researchers are concerned to have some indication of the importance of the particle drag law expression. The rather large swelling coefficient of the base case was necessary to achieve a satisfactory particle burn out with the model of Field et al (24). Clearly a burn out model allowing a more realistic value is a desirable goal. The remaining studies are ones also chosen because of their interest to furnace designers and modellers.

Although the effect of the various alterations can be examined with reference to the many predicted quantities the number of graphs and amount of information would be excessive. We have chosen to compare only the wall heat transfer, a parameter of interest to the engineer and a generally useful one for characterizing the many combustor performance criteria.

Table II Specifications of Basic Operating Conditions*

	CCRL Predictions, swirl setting 3 (base case)	Sensitivity Studies (base case)
Fuel flow rate (kg/hr)	64 (wet with 7.8% H_2O)	65
Primary air flow rate (kg/hr)	360	237
Secondary flow rate (kg/hr)	335	553
Excess air	34%	30%
Primary air ratio (% total)	51.8%	30%
Primary air velocity (m/s)	13.9	9.34
Secondary air velocity (m/s)	10.5	20.9
Primary air temperature (^{o}C)	75	82
Secondary air temperature (^{o}C)	169	259
Swirl number	0.25	0.25
Wall temperature (^{o}C)	137	727
Wall emissivity	0.6	0.6
Particle size distribution	31.7% by mass of 40.5 µm, 55% of 59 µm, 10% of 89.5 µm, 3.3% of 155 µm	50% by mass of 35 µm 10% of 55 µm and 40% of 100 µm
Thermal heat input (GJ/hr)	1.676	1.8
Swelling coefficient of coal	4.0	4.0
Scattering coefficient	0.9	0.9

*Base case modelling information

- Devolatilization model; Baum and Street (16)
- Char burn out model; Field et al (24)

Table III: Conditions for Sensitivity Studies

Type of study and sensitivity parameter	Details
1. Drag law: drag coefficient, C_d	Case I; C_d (run 1)*
	Case II; 1.1 C_d (run 2)
2. Radiation sensitivity studies	
a. Absorption; absorption coefficient	Case I; K_{total} (run 1)
	Case II; 2.0 k_{total} (run 3)
b. Scattering; scattering coefficient, f	Case I; f = 0.9 (run 1)
	Case II; f = 0.0 (run 4)
3. Particle swelling; swelling index, SW	Case I; SW = 4.0 (run 1)
	Case II; SW = 1.1 (run 5)
	Case III; SW = 1.0 (run 6)
4. Wall temperature; TW	Case I; TW = 1000^{o}K (run 1)
	Case II; TW = 1100^{o}K (run 8)
5. Wall emissivity; ϵ_w	Case I; TW = 1100^{o}K, ϵ_w = 0.8 (run 7)
	Case II; TW = 1100^{o}K, ϵ_w = 0.6 (run 8)
6. Char burn out models	Case I; Field et al model (run 1)
	Case II; Mitchell and McLean model (run 9)
7. Devolatilization models	Case I; Baum and Street (run 1)
	Case II; Anthony et al (run 10)
	Case III; Single reaction model (run 11)
	Case IV; Kobayashi et al (run 12)

*Run 1 is the base case for sensitivity studies for the operating conditions of Table II.

Table IV Modelling Conditions for CCRL Tunnel Furnace Comparison*

Run No.	Char burn out model	Devolatilization model
1 (base case)	Field et al	Baum and Street
2	Mitchell and McLean	Baum and Street

*These runs are for the operating conditions of table II for CCRL furnace.

Effect of Drag Coefficient

The effect on the heat transfer to the cylindrical walls of a 10% increase in the drag coefficient is shown in Fig. 4. The total radiative heat transfer (which accounts for almost all of the total heat transfer in this combustor) is augmented by 3%, rather more than was expected. The largest effect of about 10% occurs near the burner where the 'slip velocity' between particles and gas is largest. The reduced slip for the higher drag case reduces the oxygen mass transfer to the particle and so reduces the burning rate and particle temperature. Because the average temperature of the combustor contents is a little higher for the increased drag and lower total heat transfer case for an equivalent burn out the convection heat transfer is a little larger.

Since an altered drag coefficient also implies a correspondingly altered mass transfer coefficient the sensitivity to C_D suggested by Fig. 4 will be less for consistently specified drag and mass transfer expressions. The need for this compatibility is the most important conclusion which may be drawn from this study. Not enough attention has been given to this point in previous studies.

Effect of Absorption Coefficient

The effect of doubling the absorption coefficient is displayed in Fig. 5. We see that the sensitivity to this alteration is rather small. The implication is that the CCRL combustor is essentially 'optically thick'. Larger industrial combustors will be even less sensitive to changes in the absorption coefficients. It is clear that in the majority of practical cases the coal optical properties

Good! Simulates full-scale

need not be accurately known. The effect of wall temperature and emissivity on the other hand is significant. One of the primary sources of uncertainty in calculating the heat transfer in large combustors is the lack of knowledge about the surface conditions of fouled walls.

The fact that the radiation heat transfer is less for the larger absorption coefficient is at first surprising. The explanation is that relatively more radiation is absorbed by the cooler flow regions near the wall for the higher absorption coefficient case. In the region where the flame diameter is greatest, about 1.8 m downstream, this effect is least.

Effect of Scattering

Only the ash scatters significantly. So referring to Fig. 6, near the burner the difference between assuming isotropic scattering, $f = 0$, and mainly (90%) forward scattering, $f = 0.9$ is negligible. The effect is also small near the exit where the temperature difference between the particles and the walls is small. At intermediate distances the effect is more significant than we had expected.

Effect of Swelling

Figure 7 confirms the expected strong effect of the particle swelling behaviour on the combustor performance. The swelling factor of unity, which is far more realistic than one of four, results in an unrealistic carbon burn out of only 52%. The predictions of these sensitivity studies are based on the model of Field et al (24).

Baum and Street (16) suggested the artefact of augmenting the swelling coefficient to achieve a correct simulation of particle burn out. An improved model which does not require such an adjustment is clearly desirable. The effect of 10% swelling, which might reasonably occur in practice, is small. As we shall see below, the Mitchell and McLean burn out model gives a reasonable simulation of events for an assumed swelling of 10%.

Effects of Wall Temperature and Emissivities

Figure 8 shows that the effect of wall temperature is much more important than that of the absorption coefficient of the combustor contents for elevated wall temperatures. This is one reason why operators of coal-fired power stations are so concerned about the fouling of heat transfer surfaces. The effect of wall emissivity is somewhat less important. Since fouled surfaces are characterized by rather low values (typically $\varepsilon_w = 0.5$ as opposed to 0.9 for clean surfaces) the value of ε_w will also play an important role at lower wall temperatures because reflection by the wall will retain its significance even though direct emission by the wall does not.

Effect of Char Burn Out Model

The difference between the two chosen char burn out models is exemplified in Fig. 9. The descrepancy is certainly large enough to give cause for concern. Because we cannot here make comparisons

with CCRL data as it is impossible to ascertain which is preferable. The previous Imperial College experience has all been for the Field et al (24) proposals, devised for British bituminous coal the performance of which when compared with data has been quite rewarding. There may be some overall advantage to the simpler but newer proposals of Mitchell et al, devised we should again note of Millmerran (Aus) bituminous coals, but more predictive experience is required to learn broadly how it can best be deployed for coal types other than that for which it is proposed. This constitutes a useful future task.

Effect of Devolatilization Model

Our previous experience has been limited to the proposal of Baum and Street (16). Figure 10 shows wall heat transfer predictions for this model and the three more recent ones, all of which are described above. The method of Anthony et al gives results which are not too different from those of Baum and Street. Because of our past successes with the Baum and Street formulation (4, 7) we are forced to conclude that the models of Kabayashi and Badzioch et al are not satisfactory in their present form.

These last two models require higher temperatures to initiate devolatilization, and it is this which is here responsible for their strange behaviours. It might be that were the upstream portion of the furnace to be refractory, as in the actual CCRL furnace, or at a temperature higher than 1100°K. the performance of these two models would be better. Certaintly it is possible to

adjust this empirical parameter so that they would conform better with the Baum and Street standard but we have preferred to retain the recommendations of their proposers.

Comparison with CCRL Data

Figure 11 compares the predicted incident wall radiation flux with the CCRL data for the operating conditions of Table II. Generally the base case predictions are not too bad, but the underprediction of the incident flux near the back end of the furnace is more than we would have expected from previous experience. Our previous experience has been with the Field et al (24) char burn out model of the base case, constructed around data for British bituminous coals. The more recent model of Mitchel et al (29) is based on data for the Australian Millmerran bituminous coal and it is at least encouraging to see that the difference in the predictions for these two proposals is not great. This leads one to conclude that they should be reasonably satisfactory for the present Alberta ~~Galt~~ bituminous coal.

Figure 12 displays comparisons between the predicted and measured temperature profiles. Two sets of data points appear due to furnace flow asymmetry. We have of course modelled the flow axisymmetrically. The predictions are for the base case. The agreement is excellent. The flatness of the profiles, given the nature of the furnace, was for the authors somewhat unexpected. When one speaks of the temperature of a two phase flow there is an ambiguity as to where the temperature of one or the other of the phases, or some mixed mean value, is meant. The present predictions are for the gas temperature

The particle temperatures are initially lower, then rise to about 50°C greater than the gas, near the exit the temperatures of the spent particles are the same as those of the gas.

Corresponding comparison of the predicted and measured oxygen profiles are presented in Fig. 13. The descrepancies are larger than for temperature, this is surprising since the two are closely linked. Data further downstream than 2.2 m are not available. If they were they could be used to check the burn out. The trend of the two comparisons of Fig. 13 does however suggest that the measured and predicted burn outs would be comparable.

Figure 14 shows predicted contours of the temperatures and the oxygen concentration. These display expected behaviours. They are given here for completeness. The O_2 contours suggest that burn out is more or less complete about 1.5 m downstream.

CONCLUSIONS

- A prediction procedure has been developed for the CCPL tunnel furnace for coal firing.
- Modifications are incorporated in the particle tracking subcode of this procedure which significantly enhance its computer economy relative to earlier codes.
- We have explored several recommendations for various elements of the physical modelling.
- We conclude that the base case model (Table IV), which has formed the basis of many previous predictions, offers a reasonable simulation of the CCPL furnace fired with a Alberta bituminous coal.

- However, since individual devolatilization and char burn out models have been developed with reference to particular coals there is a need to explore further the universality of these recommendations. Obviously it would be totally unpractical to have to employ different model constants for each coal type. Thus far we have shown that a useful degree of universality seems to be contained by the best of the present devolatilization and char burn out models.
- The devolatilization and char burn out phenomena appear to be the critical ones for pulverized coal modelling. They depend on many complex factors and have so far been insufficiently explored.
- The immediate future task is to make many more predictions of the CCRL furnace for conditions for which data are available in order to explore further the generality and validity of the current model proposals. The outcome will be experience on how to procure predictions of the best quality, and the isolation of specific further model defects.
- On the whole, the predictions of the one CCRL data set we have considered have been fairly good.
- They are good enough to allow the present predictive tool to be used to explore the performance of the CCRL tunnel furnace for operating conditions for which measurements are not currently available.

NOMENCLATURE

A, A'	cross-sectional area
A_p	total projected area of particles per unit volume
B	devolatilization rate constant
B_1, B_2	frequency factors
C_1, C_2, C_3, C_4	empirical constants
C_D	drag coefficient
C_p	particle specific heat
$C_{\varepsilon 1}, C_{\varepsilon 2}, C_\mu$	empirical constants
D_c	diffusion constant
d, d_p	particle diameter
E	activation energy and emissive power
E_o	mean activation energy
E_1, E_2	activation energies of competing reactions
E_i	activation energy of a reaction i
F_{ox}	volume fraction of oxygen
f	mixture fraction, scattering coefficient
$f(E)$	gaussian distribution function for activation energy
G	mass flow rate
H_b	heat transfer to the particle per unit mass due to burning
H_c	convective heat transfer to the particle per unit mass
H_r	heat transfer to unit mass of particle due to radiation
H_t	total heat transfer to the particle per unit mass
I	intensity of thermal radiation
K, K_1, K_2, K_i	Arrhenius rate constants
K_T	$(\equiv \frac{K_{ch} \cdot K_{ph}}{K_{ch} + K_{ph}})$ overall rate coefficient
k	absorption coefficient and turbulent kinetic energy

K_{ph}, K_{ch}	diffusion and chemical rate coefficients
K_g	gas thermal conductivity
L	latent heat of devolatilization
M	total flux (convective plus diffusive)
M_c	atomic weight of carbon
M_p	particle mass
ΔM_p	mass flux into gas phase due to the particle
M_u	u-directed momentum
M_ϕ	a scalar quantity
m	mass fraction
Nu	Nusselt number
n	reaction order and distance normal to the wall
P	turbulence production
p	pressure
$p(\Omega,\Omega')$	probability of incident radiation in the direction Ω' being scattered into the element of solid angle $d\Omega$
R	universal-gas constant
R_c	particle burning rate
Re	Reynolds number
R_{fu}	volumetric reaction rate of fuel
r	radial co-ordinate and reflectively
r_w	wall reflectivity
S	source term
SW	swelling coefficient
s	stoichiometric oxygen requirement per unit mass of fuel
s_Ω	distance in the direction of radiation intensity I
T	temperature
t	time

Δt	small time step
U_{diff}	particle diffusion velocity, axial-direction
u	x-direction velocity
V	mass of volatiles evolved/mass of original coal
V^*	the value of V at $t \to \infty$
V_θ	tangential velocity
V_{diff}	particle diffusion velocity in r-direction
v	r-direction velocity
X_v	fraction of volatiles released
x,z	axial co-ordinate
ψ'	surface factor
ε	rate of dissipation of k and emissivity
ε_w	wall emissivity
ϕ	any property and a function
ϕ'	mechanism factor
σ_ϕ	empirical constant
μ	viscosity
μ_{eff}	effective viscosity
μ_t	turbulent viscosity
σ	Stefan-Boltzmann constant and standard deviation of activation energy
α_1,α_2	volatile yield of two competing reactions

Subscripts

n	north
s	south
e	east
w	west
g	gas

p	particle
fu	fuel
ox	oxidant
pr	product

Superscripts

'	fluctuating value
-	time-mean value

REFERENCES

1. Gosman, A.D., Lockwood, F.C. and Salooja, A.P. The prediction of cylindrical furnaces gaseous fueled with premixed and diffusion burners. Proceedings of 17th Symposium (International) on Combustion, p. 747, Leeds, Aug. 1978.

2. Gosman, A.D., Lockwood, F.C., Megahed, I.E.A. and Shah, N.G. The prediction of the flow, reaction and heat transfer in the combustion of a glass furnace. Proceedings AIAA Aerospace Sciences Meeting, Paper 80-0016, Pasadena, California, Jan. 1980. Journal of Energy, Vol. 6, No. 6, pp. 353-360, 1982.

3. Lockwood, F.C., Salooja, A.P. and Syed, S.A. A prediction method for coal-fired furnaces. Combustion and Flame, Vol. 38, No.1, pp. 1-15, 1980.

4. Lockwood, F.C. and Salooja, A.P. The prediction of the combustion and heat transfer from a P.F. flame in a cement kiln. International Flame Research Foundation, Doc. nr. F 21/xa/43, Oct. 1979.

5. Lockwood, F.C. and Salooja, A.P. The prediction of some furnace pulverised bituminous coal flames. Imperial College, Mech. Eng. Dept., Fluids Section Report FS/82/3. To appear in Combustion and Flame.

6. Lockwood, F.C. and Salooja, A.P. Prediction of long pulverized coal flames. Presented at Joint Meeting of Pulverized Coal and Flame Chemistry Panels of IFRF, Houillere de Provence, Oct. 1981, IFRF Doc. nr. F 22/ca/42.

7. Launder, B.E. and Spalding, D.B. Mathematical Models of Turbulence. Academic, New York, 1972.

8. Smith, P.J., Fletcher, T.H. and Smoot, L.D. Model for pulverized coal fired reactors. Eighteenth Symposium (International) on Combustion. The Combustion Institute, Pittsburgh, PA, 1980.

9. Lockwood, F.C. and Naguib, A.S. The prediction of the fluctuations in the properties of free, round-jet, turbulent diffusion flames. Combustion and Flame, Vol. 24, pp. 109-124, 1975.

10. Spalding, D.B. The calculations of combustion processes. Imperial College, Mech. Eng. Dept. Rept. RF/TN/A/7, 1971.

11. Medgal, D. and Agosta, V.D. Appl. Mech. 35, 860-865, 1967.

12. Crowe, C.T. A computational model for the gas droplet flow field in the vicinity of an atomizer. Western States Section, The Combustion Institute, Paper No. 74-25, 1974.

13. Hassan, M.M. and Lockwood, F.C. Predicting particle motion in turbulent flows. Doc. nr. F 21/ca/45, Pulverized Fuel and Aerodynamics Panels, 23 and 24 September 1980, Gummersbach, Germany.

14. Abbas, A.S., Koussa, S.S. and Lockwood, F.C. The prediction of a variety of heavy oil flames. Proceedings of ASME Winter Annual Meeting, Special Session on Two Phase Combustion Liquid Fuels, Washington, Nov. 1981.

15. Abbas, A.S., Koussa, S.S. and Lockwood, F.C. The prediction of particle laden gas flows. Proceedings of 18th Symposium (International) on Combustion, Combustion Institute, Waterloo, Canada, 1980.

16. Baum, M.M. and Street, P.J. Combustion Science and Technology, 3, pp. 231-243, 1971.

17. Lockwood, F.C., Rizvi, S.M.A. and Shah, N.G. Some predictive experiences of coal firing. Presented at Combustion Institute Meeting, Central States Section, on the Combustion of Coal and Other Non-Petroleum Fuels, Lexington, Kentucky, March 1983.

18. Badzioch, S. and Hawksley, P.G.W. Kinetics of thermal decomposition of pulverized coal particles. Ind. Eng. Chem., Process Design Develop., 9, 521, 1970.

19. Anthony, D.B., Howard, J.B., Hottel, H.C. and Meissner, H.P. Rapid devolatilization and hydrogasification of bituminous coal. Fuel, 55, 121, 1976.

20. Anthony, D.B., Howard, J.B., Hottel, H.C. and Meissner, H.P. Rapid devolatilization of pulverized coal. Fifteenth Symposium (International) on Combustion, p. 1303, The Combustion Institute, Pittsburgh, Pa., 1975.

21. Kobayashi, H., Howard, J.B. and Sarofim, A.F. Coal devolatilization at high temperatures. Sixteenth Symposium (International) on Combustion. The Combustion Institute, Pittsburgh, 411, 1977.

22. Magnussen, B.F. and Hjertager, H. Sixteenth Symposium (International) on Combustion, The Combustion Institute, Pittsburgh, PA, p. 719, 1976.

23. Spalding, D.B. Thirteenth Symposium (International) on Combustion, The Combustion Institute, Pittsburgh, PA, p. 649, 1971.

24. Field, M.A., Gill, D.W., Morgan, B.B. and Hawksley, P.G.W. Combustion of pulverized coal. The British Coal Utilisation Research Association, Leatherhead, 1967.

25. Nettleton, M.A. Temperature measurements on burning coal particles in radiating enclosure. Combustion and Flame, 311, 1965.

26. Ayling, A.B. and Smith, I.W. Measured temperatures of burning pulverized-fuel particles, and nature of the primary reaction product. Combustion and Flame, 18, 173, 1972.

27. Seeker, W.R., Samuelsen, G.S., Heap, M.P. and Tralinger, J.D. Eighteenth Symposium (International) on Combustion, p. 1213, The Combustion Institute, Pittsburgh, PA, 1981.

28. Smith, I.W. The combustion rates of coal chars: A review. Nineteenth Symposium (International) on Combustion, The Combustion Institute, 1982.

29. Mitchell, R.E. and McLean, W.J. On the temperature and reaction rate of burning pulverized fuels. Nineteenth Symposium (International) on Combustion, The Combustion Institute, 1982.

30. Gibb, J. Central Electricity Generating Board, Southampton, England, Private Communication, 1977.

Fig. 1

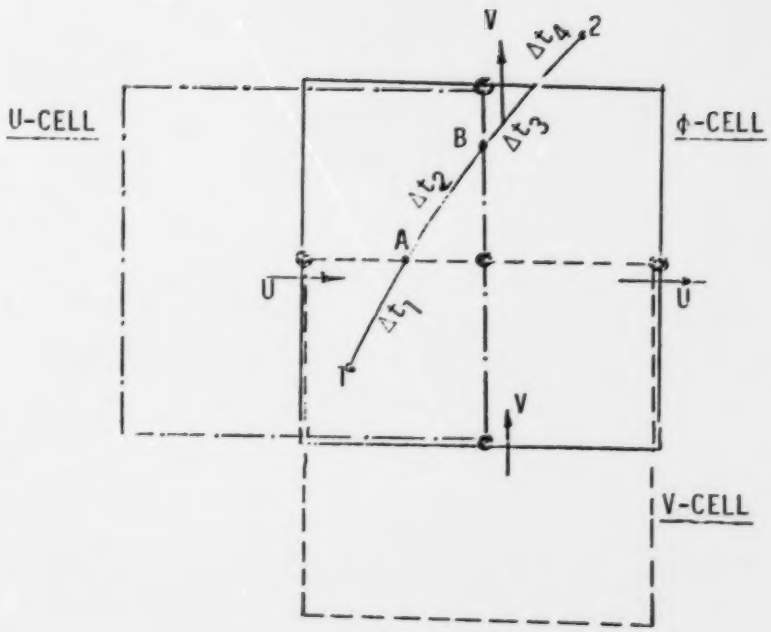

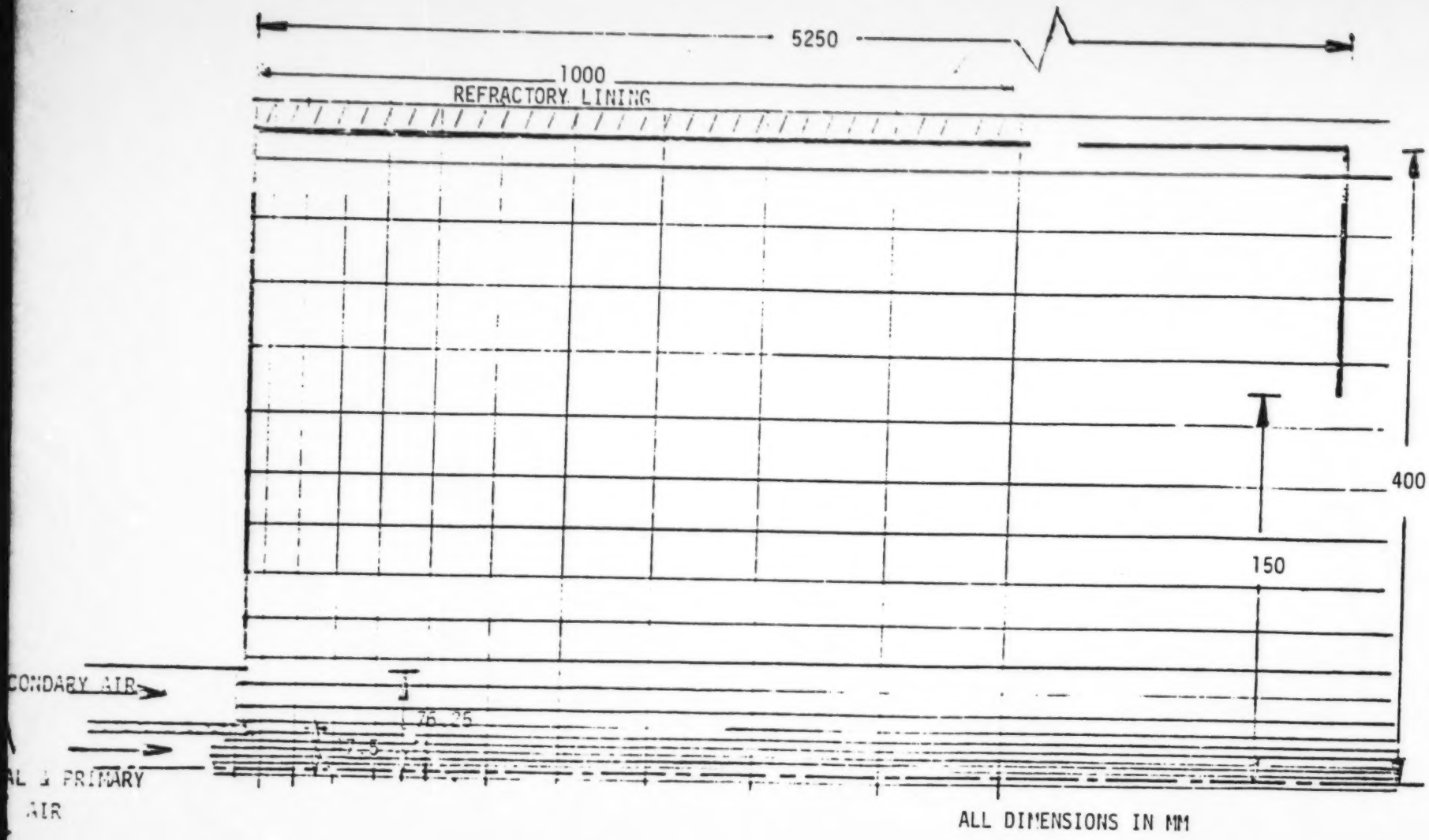
5250
1000
REFRACTORY LINING
400
150
CONDARY AIR
AL & PRIMARY
AIR
ALL DIMENSIONS IN MM

Fig. 2

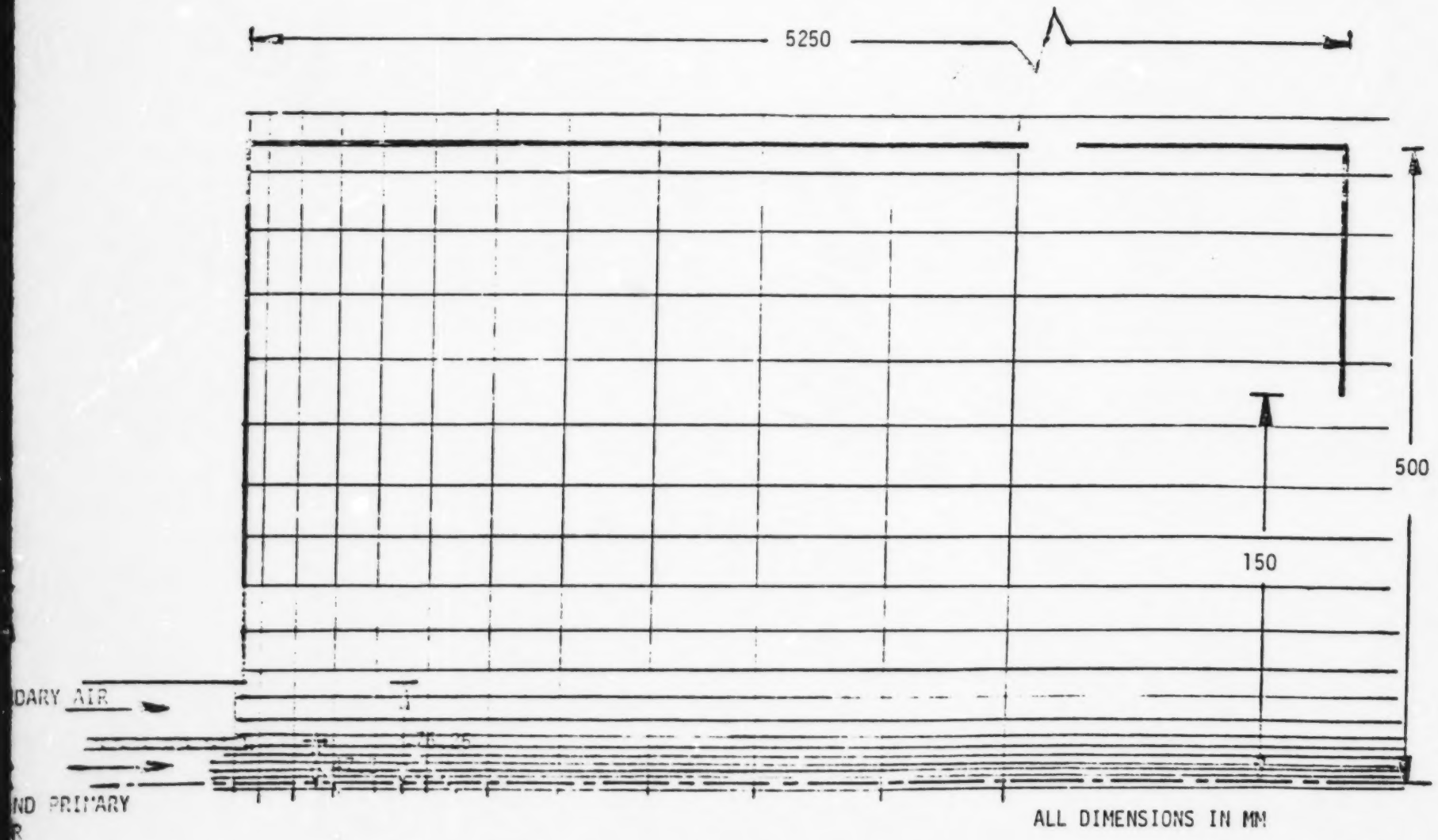

Fig. 3

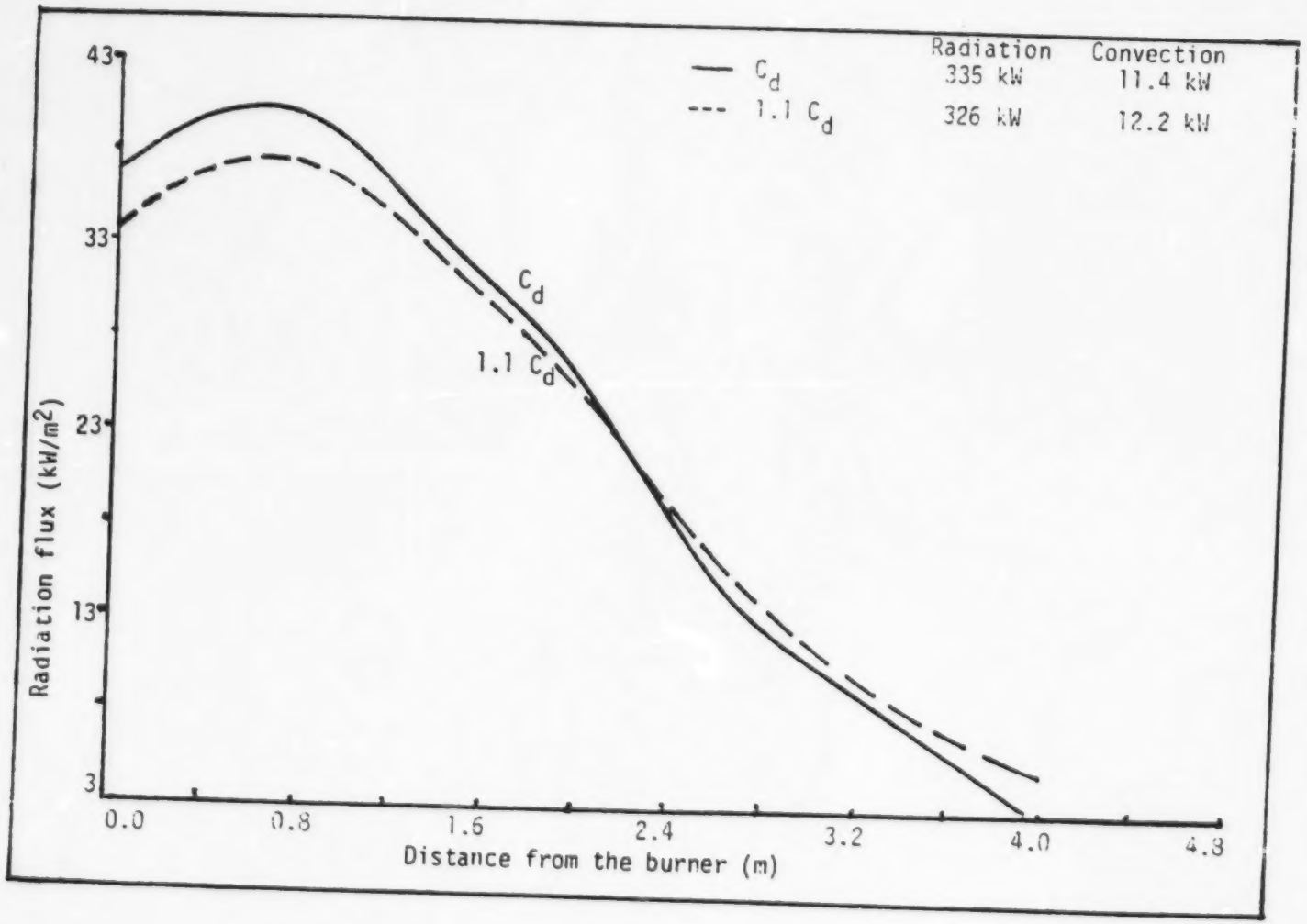
Radiation
Convection
— C_d
335 kW
11.4 kW
--- 1.1 C_d
326 kW
12.2 kW
43
33
23
13
3
C_d
1.1 C_d
Radiation flux (kW/m²)
0.0
0.8
1.6
2.4
3.2
4.0
4.8
Distance from the burner (m)

Fig. 4

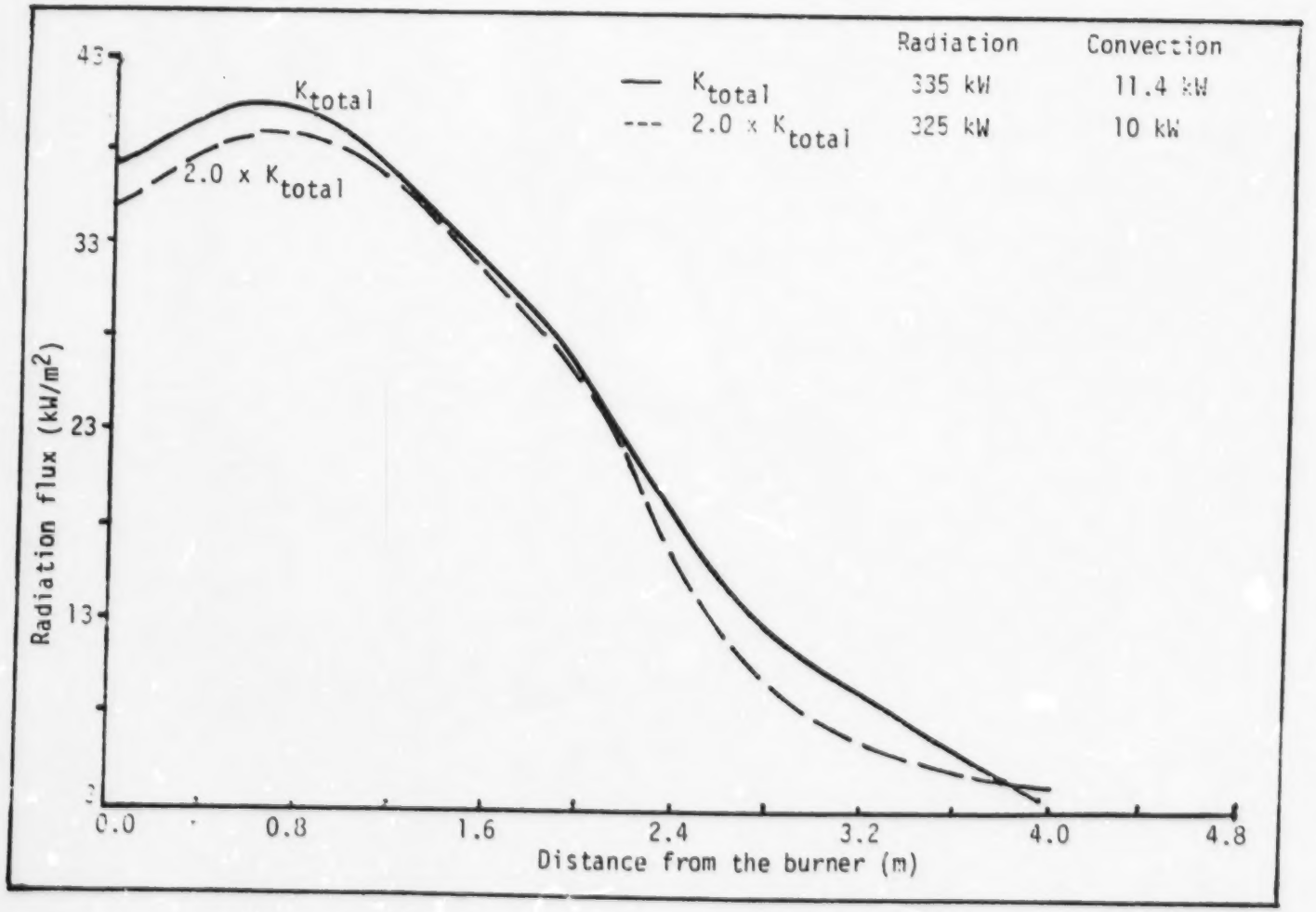
Radiation
Convection
K_{total}
335 kW
11.4 kW
2.0 x K_{total}
325 kW
10 kW
K_{total}
2.0 x K_{total}
43
33
23
13
Radiation flux (kW/m²)
0.0
0.8
1.6
2.4
3.2
4.0
4.8
Distance from the burner (m)

Fig. 5

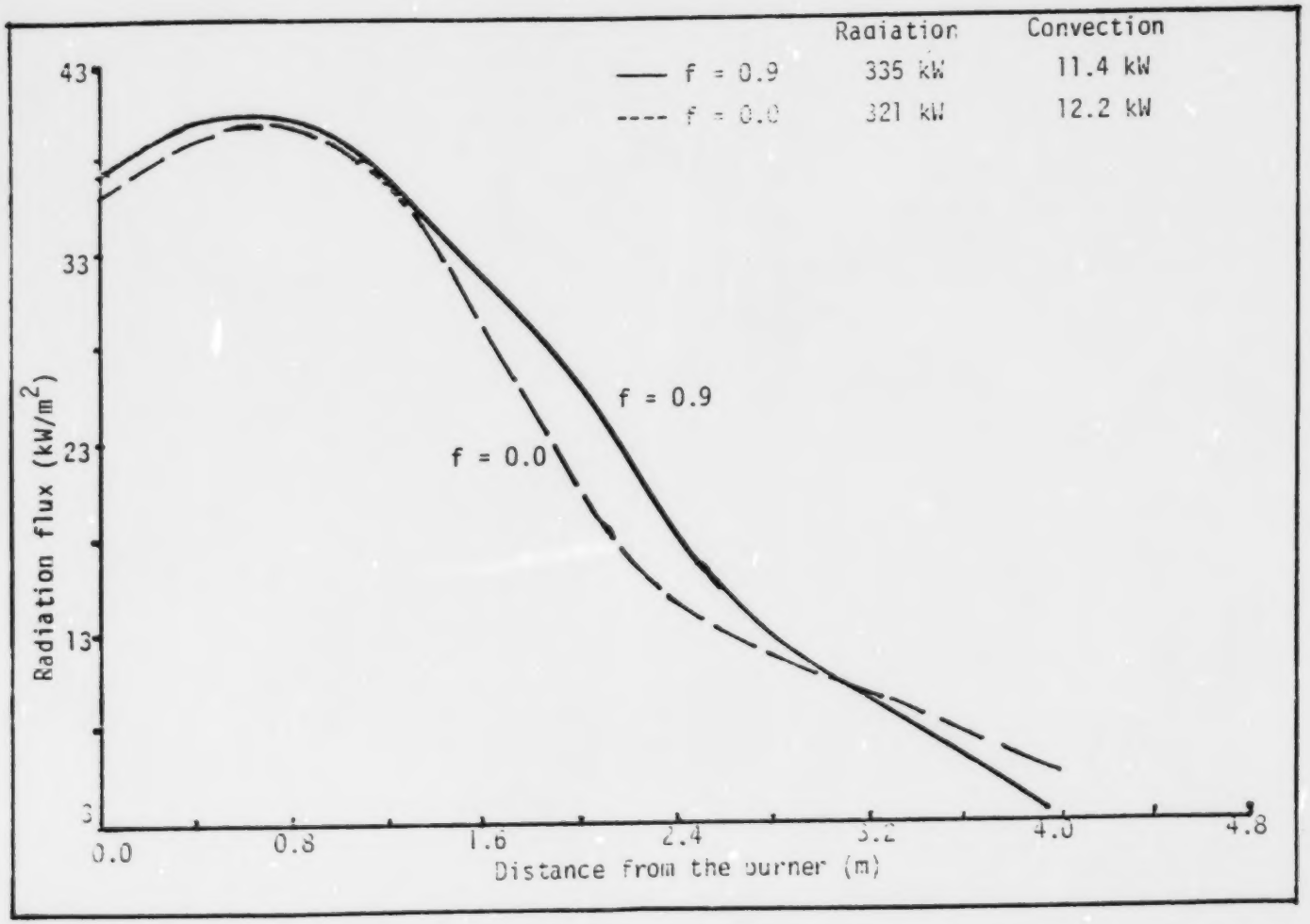
Radiation
Convection
—— f = 0.9
335 kW
11.4 kW
---- f = 0.0
321 kW
12.2 kW
43
33
23
13
3
Radiation flux (kW/m²)
f = 0.9
f = 0.0
0.0
0.8
1.6
2.4
3.2
4.0
4.8
Distance from the burner (m)

Fig. 6

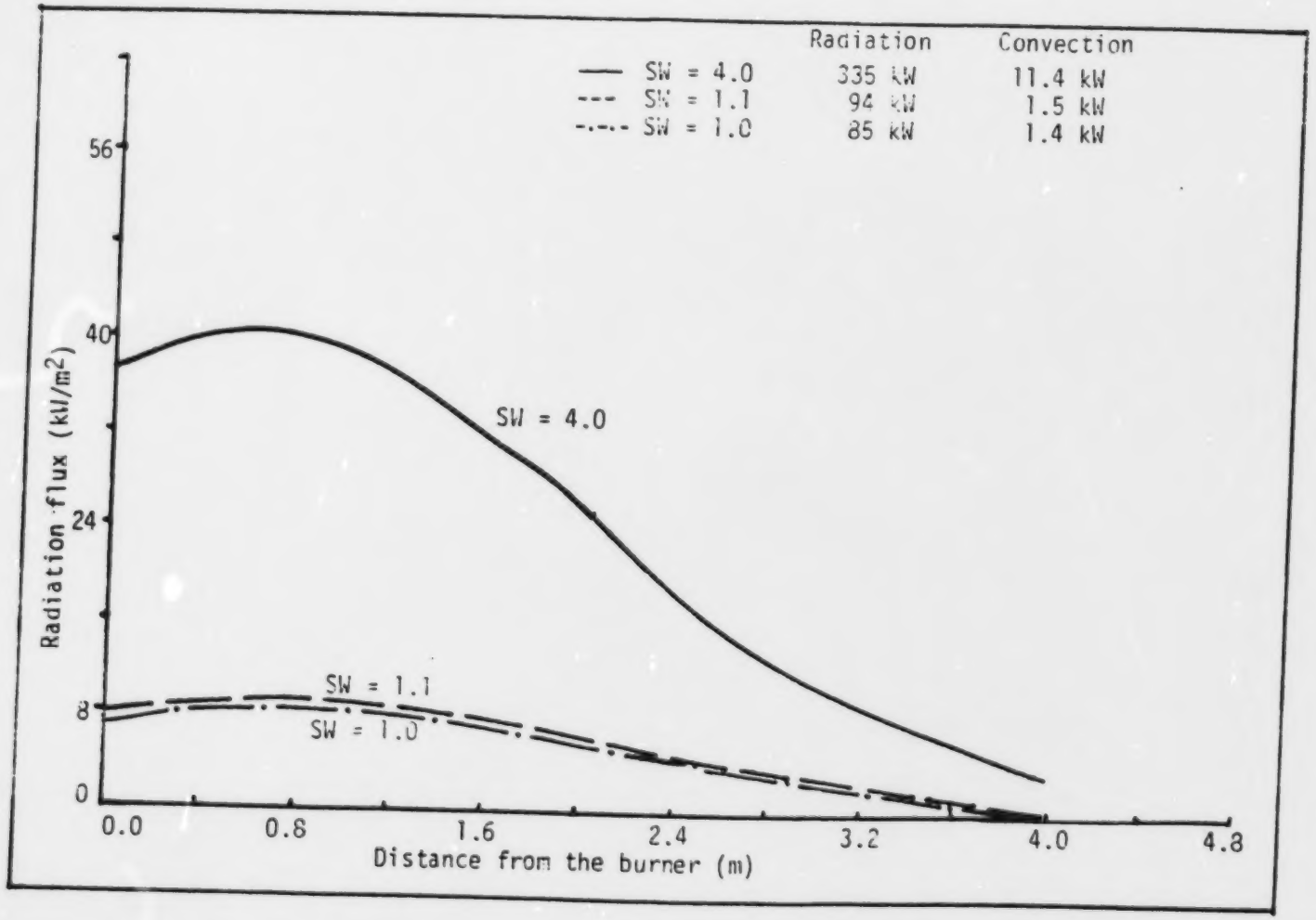
Radiation
Convection
SW = 4.0
335 kW
11.4 kW
SW = 1.1
94 kW
1.5 kW
SW = 1.0
85 kW
1.4 kW
56
40
24
8
0
Radiation flux (kW/m²)
SW = 4.0
SW = 1.1
SW = 1.0
0.0
0.8
1.6
2.4
3.2
4.0
4.8
Distance from the burner (m)

Fig. 7

Fig. 8

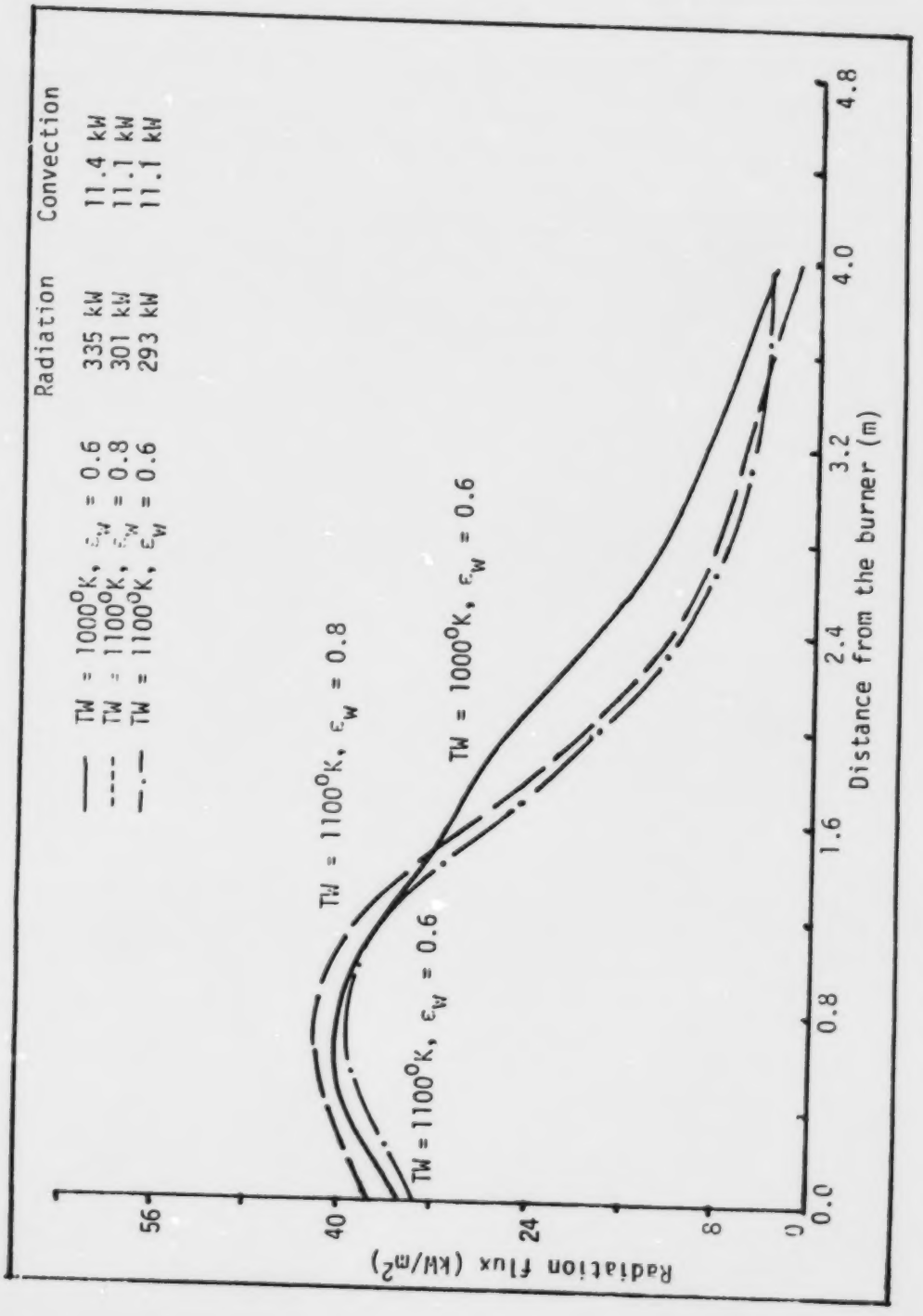
Radiation
Convection
TW = 1000°K, εw = 0.6
TW = 1100°K, εw = 0.8
TW = 1100°K, εw = 0.6
335 kW
301 kW
293 kW
11.4 kW
11.1 kW
11.1 kW
TW = 1100°K, εw = 0.8
TW = 1100°K, εw = 0.6
TW = 1000°K, εw = 0.6
Radiation flux (kW/m²)
Distance from the burner (m)
0
8
24
40
56
0.0
0.8
1.6
2.4
3.2
4.0
4.8

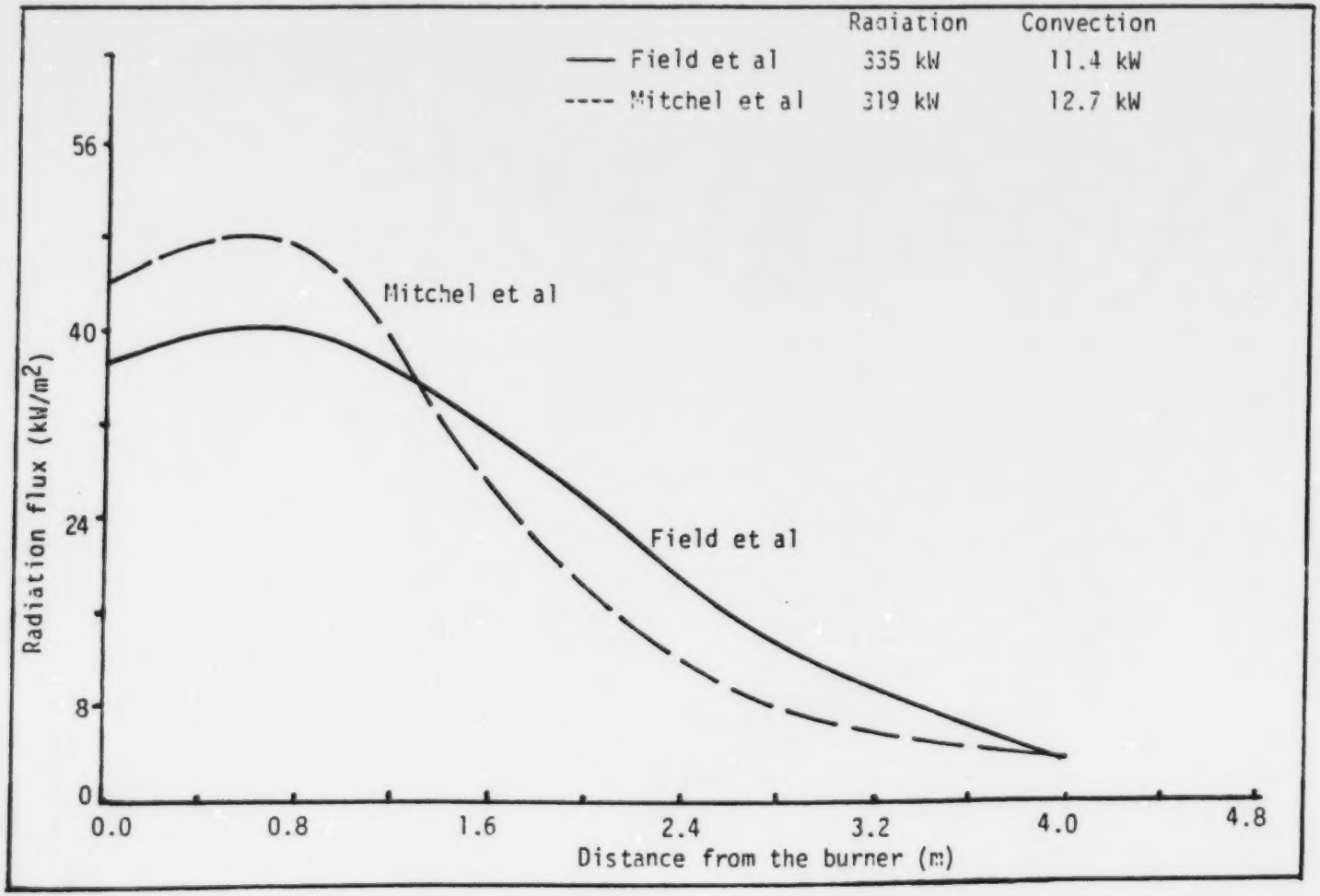
Radiation
Convection
Field et al
335 kW
11.4 kW
Mitchel et al
319 kW
12.7 kW
56
40
24
8
0
Radiation flux (kW/m2)
Mitchel et al
Field et al
0.0
0.8
1.6
2.4
3.2
4.0
4.8
Distance from the burner (m)

Fig. 9

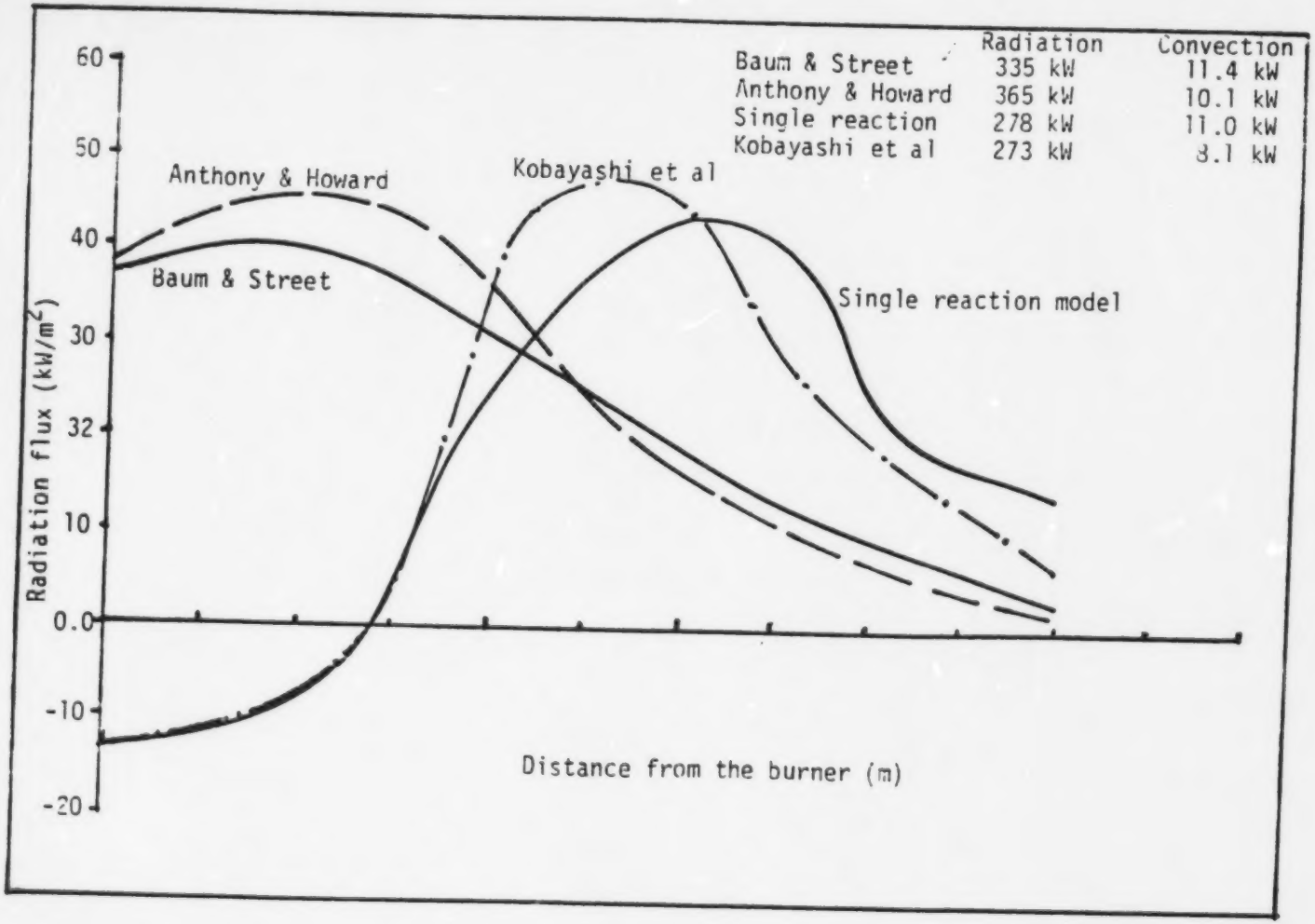
Radiation
Convection
Baum & Street 335 kW 11.4 kW
Anthony & Howard 365 kW 10.1 kW
Single reaction 278 kW 11.0 kW
Kobayashi et al 273 kW 8.1 kW
Anthony & Howard
Kobayashi et al
Baum & Street
Single reaction model
Radiation flux (kW/m²)
60
50
40
30
32
10
0.0
-10
-20
Distance from the burner (m)

Fig. 10

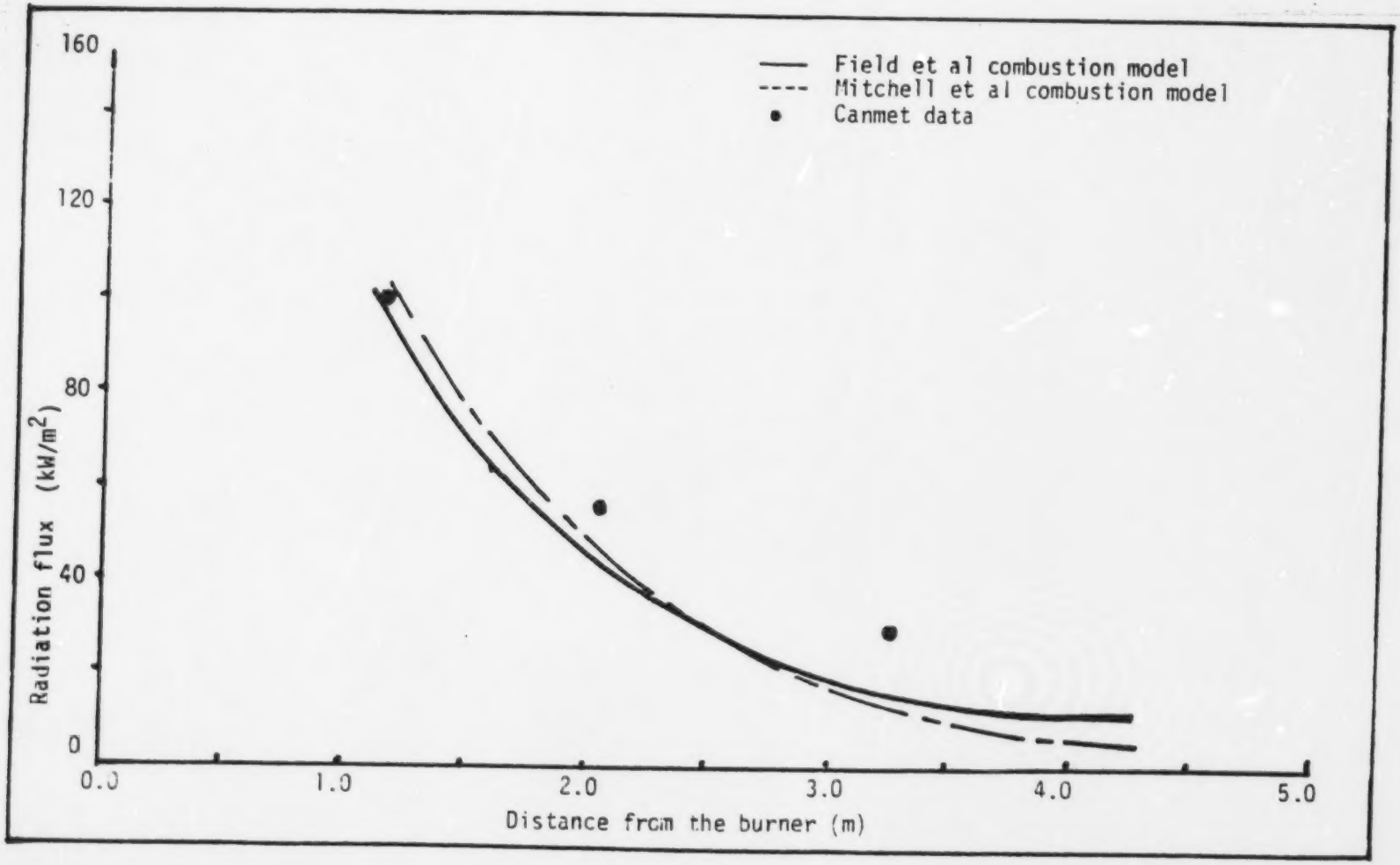
Field et al combustion model
Mitchell et al combustion model
Canmet data
160
120
80
40
0
Radiation flux (kW/m²)
0.0
1.0
2.0
3.0
4.0
5.0
Distance from the burner (m)

Fig. 11

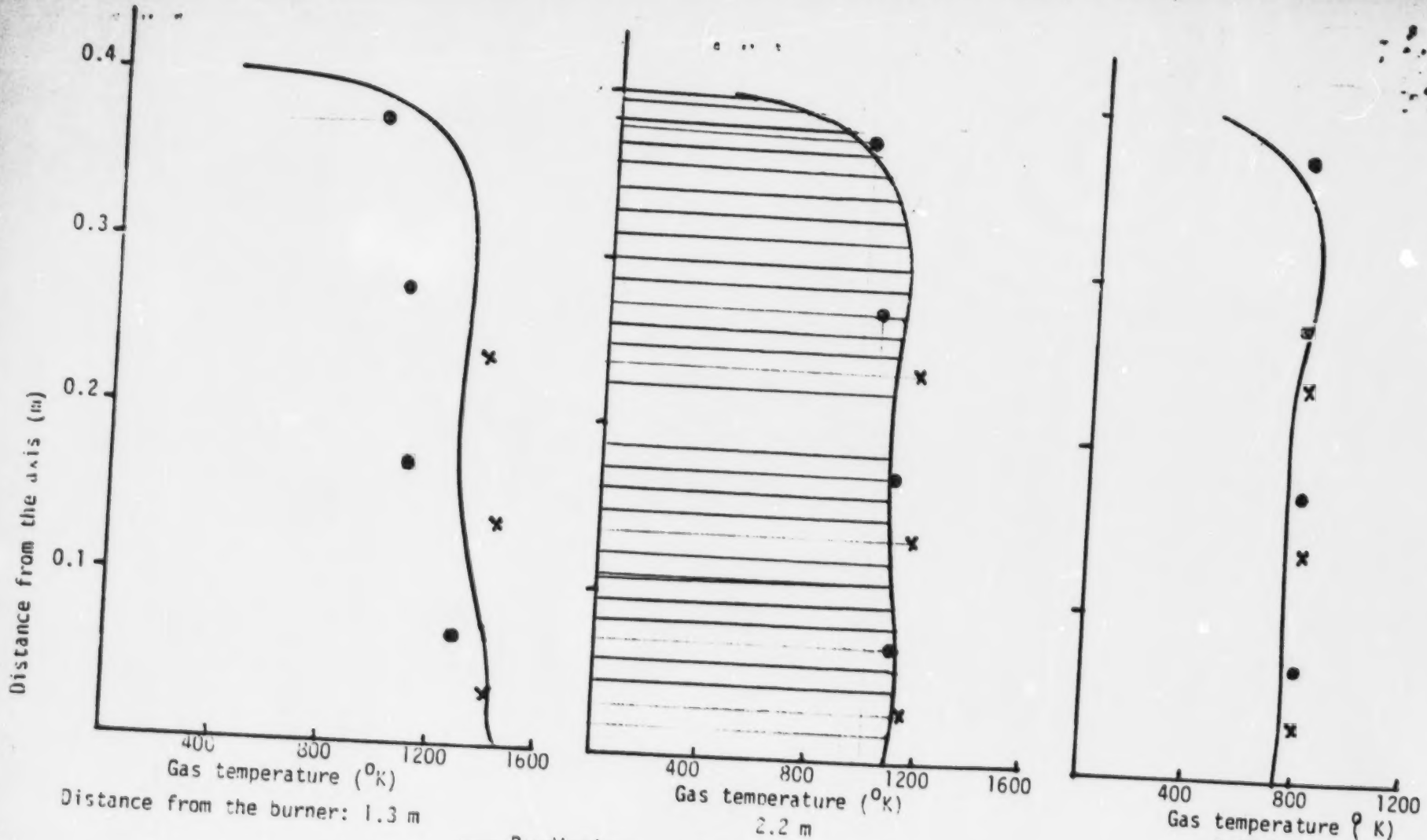
0.4
0.3
0.2
0.1
Distance from the axis (m)
400
800
1200
1600
Gas temperature (°K)
Distance from the burner: 1.3 m
Gas temperature (°K)
2.2 m
Gas temperature (° K)
5.05 m
— Predictions, • Canmet data above the axis,
x Canmet data below the axis

Fig. 12

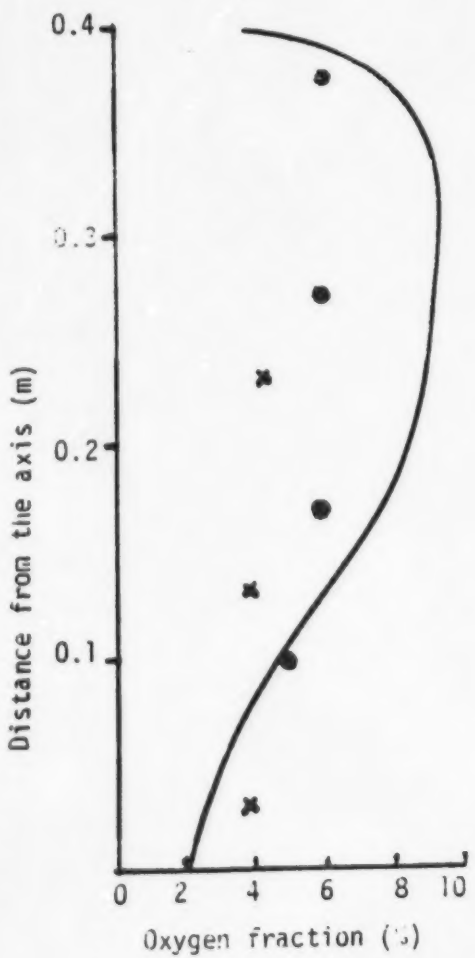

Distance from the burner: 1.3 m

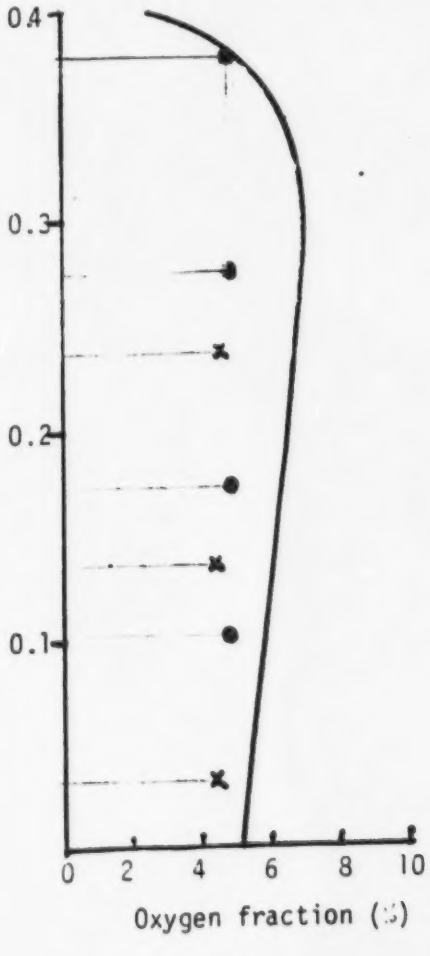

2.2 m

—— Predictions, • Canmet data above the data, x Canmet data below the axis

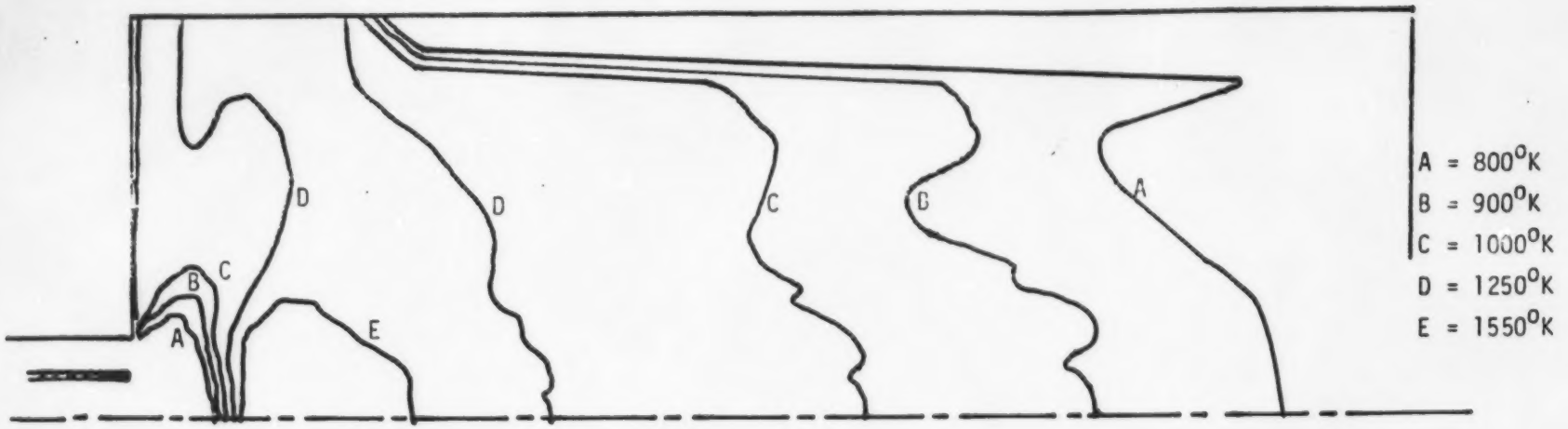

Gas temperature

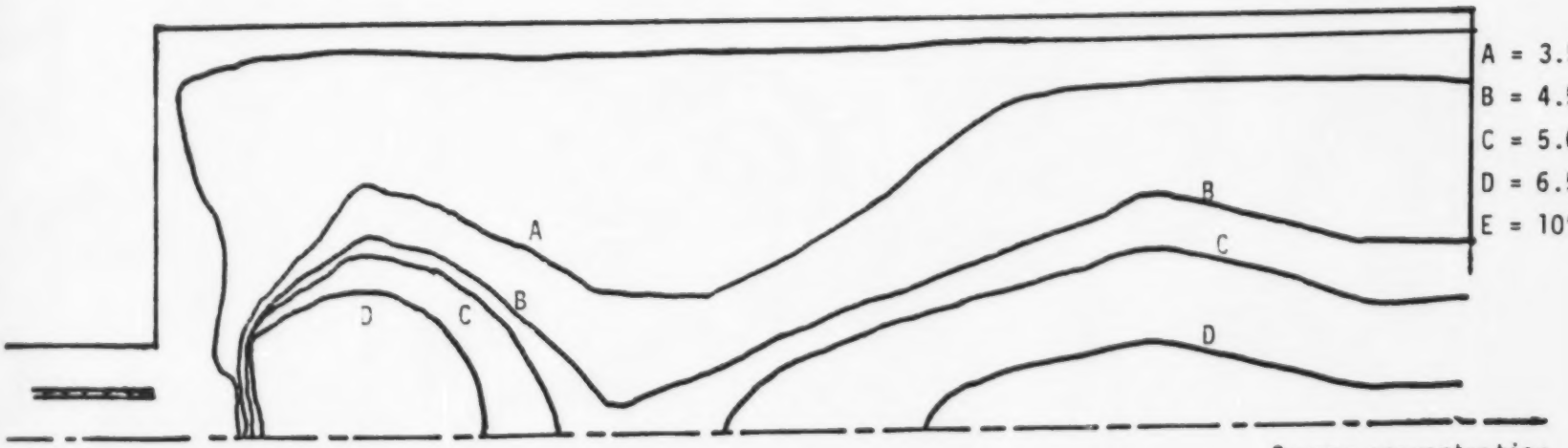

Oxygen concentration

Fig. 14